

**PLASTIC DEFORMATION OF GALLIUM ARSENIDE**

by

**IKECHUKWU UDEVI-ARUEVORU**

**M.Sc (Physics), University of Nigeria**

**Nsukka, 1983**

**B.Sc (Physics), University of Nigeria**

**Nsukka, 1980**

**A THESIS SUBMITTED IN PARTIAL FULFILLMENT OF THE REQUIREMENTS FOR**

**THE DEGREE OF MASTER OF SCIENCE**

in

**FACULTY OF GRADUATE STUDIES**

**Department of Metals and Materials Engineering**

**We accept this thesis as conforming**

**to the required standard**

---

**THE UNIVERSITY OF BRITISH COLUMBIA**

**October 1991**

**© Ikechukwu Udevi-Aruevoru**

In presenting this thesis in partial fulfilment of the requirements for an advanced degree at the University of British Columbia, I agree that the Library shall make it freely available for reference and study. I further agree that permission for extensive copying of this thesis for scholarly purposes may be granted by the head of my department or by his or her representatives. It is understood that copying or publication of this thesis for financial gain shall not be allowed without my written permission.

(Signature)

Department of METALS & MATERIALS ENGINEERING

The University of British Columbia  
Vancouver, Canada

Date 15/11/91

### **Abstract**

The present investigation was undertaken to determine the validity of Haasen's model of plastic deformation for GaAs over an extended range of temperatures and to observe the relation between the dislocation density in the deformed samples and the deformation variables. The experimental results show a discrepancy with the predictions of the model. This discrepancy and also the different values of the activation parameters reported in the literature was explained in terms of the contributions of temperature induced effects to the plastic strain rate .

The dislocation densities in the deformed samples obtained by counting dislocation etch pits indicate that the density of dislocations in deformed GaAs is directly related to the applied stress, the plastic strain rate, the test temperature while being inversely related to the applied strain rate.

## Table of Contents

Abstract .....	ii
Table of Contents .....	iii
List of Tables .....	vi
List of Figures .....	vii
Acknowledgements .....	ix
1. Introduction .....	1
1.1 Crystal Structure and Dislocations in GaAs .....	1
1.2 Stress - Strain Curves of f.c.c. Metals .....	4
1.3 Dislocations and Macroscopic Deformation Variables .....	8
2 Literature Review .....	9
2.1 Experimental Study .....	9
2.2 Theoretical Studies .....	10
2.2.1 The CRSS Model .....	10
2.2.2 Haasen's Model .....	11
2.3 The Yield Point .....	14
2.3.1 Dynamical Recovery .....	15
2.4 Application of Haasen's Model .....	16

3	Objectives .....	20
4	Experimental Procedure .....	21
4.1	Determination of The Specimen Orientation .....	21
4.2	Specimen Preparation and Testing .....	23
4.2.1	Compression Tests Specimens .....	23
4.2.2	Compression Testing Apparatus .....	23
4.2.3	Compression Testing Procedure .....	25
4.3	Tensile Tests .....	26
4.3.1	Preparation of The Tensile Tests Specimens .....	26
4.3.2	Tensile Testing Apparatus .....	27
4.3.3	Tensile Testing Procedure .....	27
4.4	Dislocation Etch Pit Density .....	30
4.4.1	Chemical Polishing .....	30
4.4.2	Etching of The Specimens .....	31
5	Observations .....	32
5.1	Compression Tests Results .....	32
5.1.1	Stress - Strain Curves .....	32
5.1.2	Temperature and Strain Rate Dependence of $m$ and $U$ .....	44

5.1.3	Dislocation Density - Compression Tests. ....	54
5.2	Tensile Tests .....	59
5.2.1	Tensile Stress - Tensile Strain Curves .....	59
5.2.2	The Temperature Dependence of The Yield Stress .....	59
5.2.3	Dislocation Density - Tensile Tests. ....	64
6	Discussion .....	70
6.1	Yield Drop .....	71
6.2	Temperature and Strain Rate Dependence of $m$ and $U$ .....	73
6.3	Stress - Strain Curves .....	78
6.3.1	Compression Tests .....	78
6.3.2	Tension Tests .....	80
6.3.3	The Relation Between The Dislocation Density and Macroscopic Deformation Variables .....	82
7	Conclusions .....	84
8	Suggestions for Further Work .....	85
	References .....	87

### List of Tables

5.1	Temperature, Yield and Recovery stresses for Series A Compression Samples. ..	40
5.2(a)	Temperature vs Yield Stress for Series B Compression Samples. ....	41
5.2(b)	Temperature vs Recovery Stress for Series B Compression Samples. ....	42
5.3	Comparison of Sample Elongations for Series B Samples. ....	43
5.4(a)	Temperature Dependence of (2+m) Values From Present Study.....	52
5.4(b)	(2+m) and $\frac{U}{(2+m)}$ Values Reported in The Literature. ....	52
5.5(a)	Temperature vs n values obtained from present study .....	53
5.5(b)	Strain Rate Dependence of $\frac{Q_{SD}}{n}$ values .....	53
5.6	Dislocation Etch Pit Densities From Series B Compression Samples. ....	55
5.7	Temperature vs Yield Stress for Tensile Tests Samples. ....	63
5.8	Dislocation Etch Pit Densities From Tensile Tests Samples.....	65
5.9	Comparison of Present Results With Results Reported in The Literature (Compression Tests).....	79

### List of Figures

1.1	α 60° Dislocations in The Shuffle Plane. ....	2
1.2	α 60° Dislocations in The Glide Plane. ....	3
1.3	Shear Stress - Shear Strain Curves for Pb Single Crystals. ....	5
1.4(a)	Temperature Dependence of The CRSS of Pb Single Crystals.....	6
1.4(b)	Flow Stress Ratio vs Temperature for Pb Single Crystals. ....	6
2.1	Comparison of Weiss's and Schroter's Results. ....	18
4.1	X-Ray Diffraction Pattern From Specimen Orientation Tests. ....	22
4.2	Compression Jig and The Tube Furnace. ....	24
4.3	Tensile Sample and The Tensile Jig. ....	29
5.1	Stress - Strain Curves From Compression Tests. ....	35
5.2	Resolved Shear Stress - Shear Strain Curves From Compression Tests. ....	36
5.3	Recovery stress from Resolved Shear Stress - Shear Strain Curves ....	37
5.4	Comparison of The Yield Stress for The Two Compression Tests Samples. ....	38
5.5	Yield Stress vs Temperature for Series B Samples. ....	39
5.6	ln of Yield Stress vs ln of Strain Rate. ....	48
5.7	ln of Yield Stress vs 1/Temperature. ....	49
5.8	ln of Recovery Stress vs 1/Temperature. ....	50

5.9	ln of Recovery Stress vs 1/Temperature. ....	51
5.10	Dislocation Etch Pits in an as Received Compression Sample .....	56
5.11	Dislocation Etch Pits in a Deformed Compression Sample .....	57
5.12	Dislocation Etch Pits in a Deformed Compression Sample .....	58
5.13	Tensile Stress - Tensile Strain Curves. ....	60
5.14	Plastic Strain at Fracture vs Temperature From Tensile Tests.....	61
5.15	Yield Stress vs Temperature From Tensile Tests.....	62
5.16	Dislocation Etch Pits in an as Received Tensile Sample. ....	66
5.17	Dislocation Etch Pits in a Deformed Tensile Sample .....	67
5.18	Dislocation Etch Pits in a Deformed Tensile Sample. ....	68
5.19	Dislocation Etch Pits in a Deformed Tensile Sample. ....	69

### **Acknowledgements**

I am grateful to my supervisors, Dr Fred Weinberg and Dr I.V. Samarasekera for their support and encouragement in the course of this work, to Johnson Matthey electronics Co. Ltd for providing the GaAs samples used in the experiments, to Bob Butters, H. Tump, Laurie Frederick and Mary Mager for their assistance and patience and finally to my colleagues in particular, to Chris Parfenuik, G. Lockhart, A. Boateng, S. Kumar, Gang Liu and C. Muojekwu for their encouragement.

## 1

**INTRODUCTION**

GaAs is a direct band gap III - V compound semiconductor which has found extensive application as substrates for electronic devices, FET transistors, lasers etc. The utility of GaAs devices is however limited by

1. A high grown - in dislocation density (usually about  $10^4$  to  $10^5$  dislocations /cm<sup>2</sup>).
2. An inhomogenous distribution of these dislocations in the material.

Dislocations have a direct effect on the electrical properties of devices because they alter the density, mobility and lifetime of electrical carriers and indirectly through their interaction with impurities and other crystalline defects. Thus dislocations in GaAs are of major importance in the technology of semiconductor devices.

**1.1 Crystal Structure and Dislocations in GaAs.**

The Bravais lattice of GaAs is f.c.c. and the crystal structure consists of alternate {111} planes of positive and negative ions which leads to a polarity in the stacking of the {111} planes. The structure may also be considered as a layered structure, each layer consisting of two {111} planes connected by three covalent bonds per atom. In contrast to f.c.c. metals, GaAs is brittle at low temperatures due to its covalent bonding and becomes increasingly plastic at temperatures above  $0.4T_m$  where  $T_m$  is the congruent melting temperature. The crystal is grown using either the Liquid Encapsulated Czochralski (LEC) technique or the Bridgeman method.

The dislocations are generated by thermoelastic stresses accompanying growth. They may also be generated in the crystal during device fabrication and in devices operating at elevated temperatures.

The dislocations in GaAs can either be positive ( $\alpha$  or  $\beta$ )  $60^\circ$  dislocations and screw dislocations. Dislocations lying between the widely spaced  $\{111\}$  planes are called the shuffle set while those lying between the narrowly spaced  $\{111\}$  planes are called the glide set. Figs 1.1 and 1.2 show the  $\alpha$   $60^\circ$  dislocations in the shuffle and glide planes respectively.

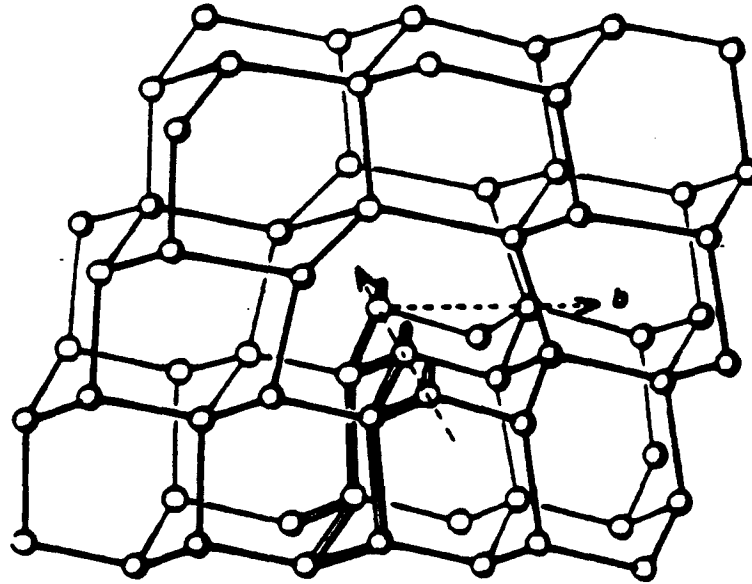


Fig. 1.1. An  $\alpha$   $60^\circ$  dislocation in the shuffle plane showing a row of dangling bonds, reference (1).

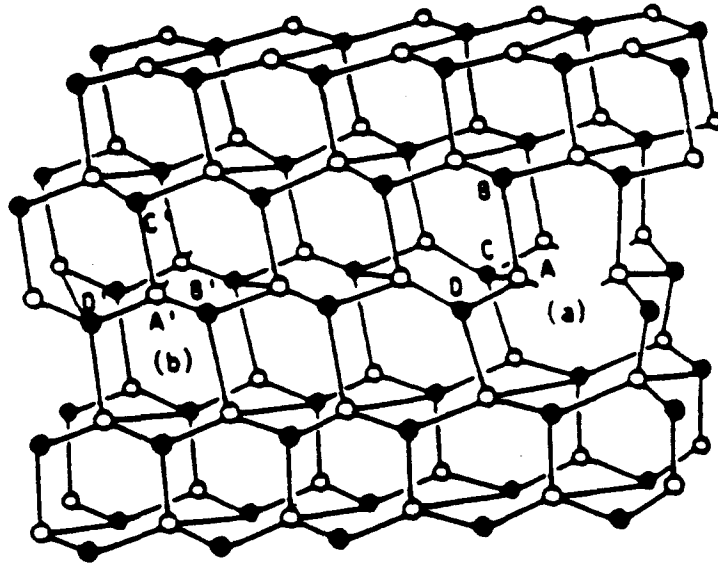


Fig 1.2 An  $\alpha$   $60^\circ$  dislocation in the glide plane, reference (1).

The dislocations contain a dense array of unpaired dangling bonds along the edge of the extra half plane of atoms. These dangling bonds are unpaired electrons and are responsible for most of the electrical properties of dislocations. Dislocation motion may occur either between two layers or between two  $\{111\}$  planes constituting a layer. Dislocations moving between two layers are referred to as the shuffle dislocations while those moving between  $\{111\}$  planes are called glide dislocations. The glide dislocation may dissociate into two Shockley partials in the same manner as in f.c.c. metals. However a direct dissociation of a shuffle dislocation into partials is difficult since this would produce dislocations with high fault energies. In addition, glide and shuffle dislocations differ in the directions of the broken bonds occurring in their cores. Dislocation climb in GaAs differs from that in f.c.c. metals. Because of its double occupancy, a jog as an elementary source of point defects produce di-vacancies on non-conservative movement. These double vacancies are less mobile than the single vacancies which is contrary to experience with f.c.c. structures.

## **1.2 Stress - Strain Curves of f.c.c. Metals.**

Although the crystal structure and dislocation properties of diamond structure materials differ from that of pure f.c.c. metals, the plastic properties of GaAs may be correlated with the corresponding behaviour of f.c.c. metals. The observed similarities in the stress - strain curves of f.c.c. and diamond structure metals and also the fact that the arrangement of dislocations as observed by a TEM study of work - hardened Ge crystals are similar to those found at corresponding points in the hardening curves of Cu, Au, and Ni - Co alloys suggests that it is the geometry of the slip planes, the interaction between the slip systems and dislocation reactions that determine the dislocation structure and work - hardening during uniaxial deformation (2).

The present investigation is concerned with the deformation of GaAs at high temperatures. There is little information or theory in the literature related to the deformation of ionic crystals such as GaAs at high temperatures. Following the premise that the plastic deformation of diamond structure semiconductors is essentially the same as that of f.c.c. metals, for which there is a large body of observations and theory, the observed plastic behaviour of GaAs can be related to the behaviour of f.c.c. metal crystals.

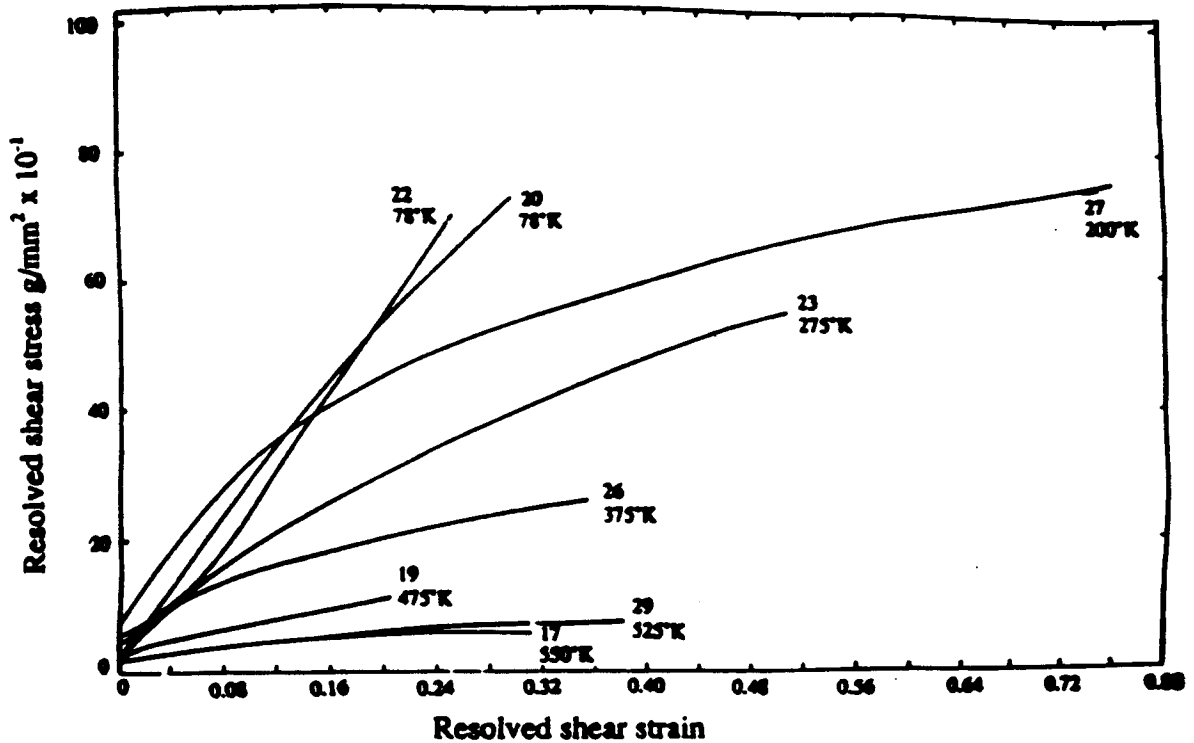


Fig. 1.3 The resolved shear stress - shear strain curves for lead single crystals, ref(3).

The deformation of f.c.c. metals at high homologous temperatures is described in an investigation of lead single crystals (3,4). Typical resolved shear stress - shear strain curves for lead in the temperature range of 78 to 550°K (0.13 to 0.92 of the melting point temperature respectively) are shown in Fig. 1.3. The onset of plastic flow decreases appreciably with increasing test temperature. The initial linear work hardening region is not clearly defined and decreases in length with increasing temperature. The major part of the deformation curve at 200°K and above, shows a progressively decreasing rate of work hardening, associated with recovery. At the highest temperatures, the maximum stresses reached are very low with very little working hardening being evident. The decrease of the CRSS with temperature for easy glide orientations is shown in Fig. 1.4(a).

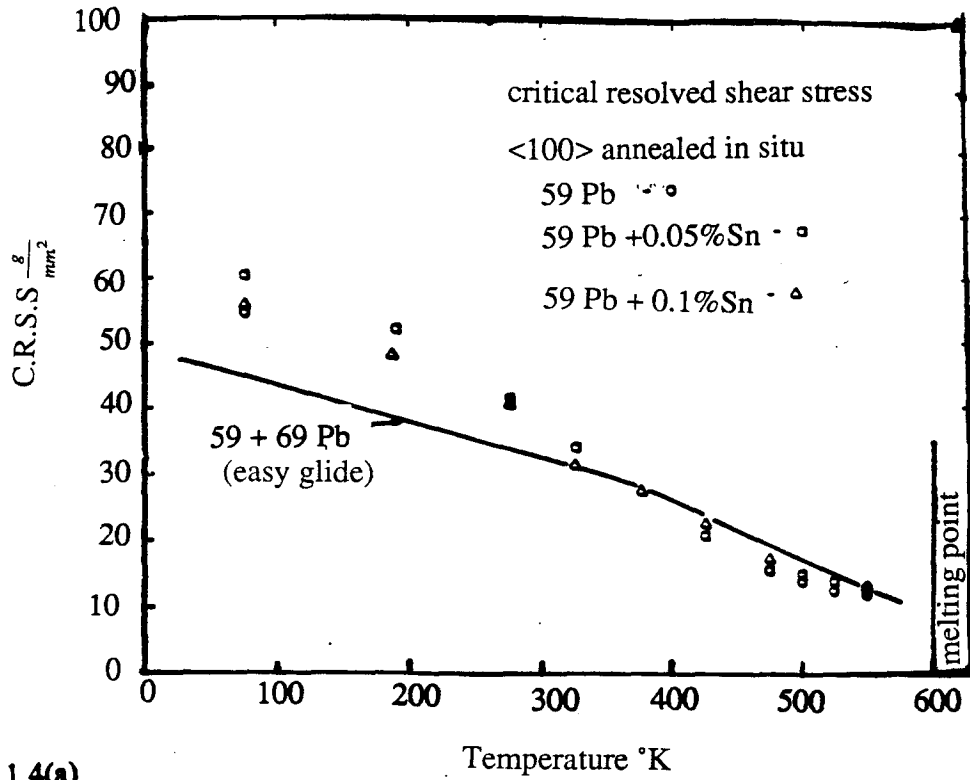


Fig. 1.4(a)

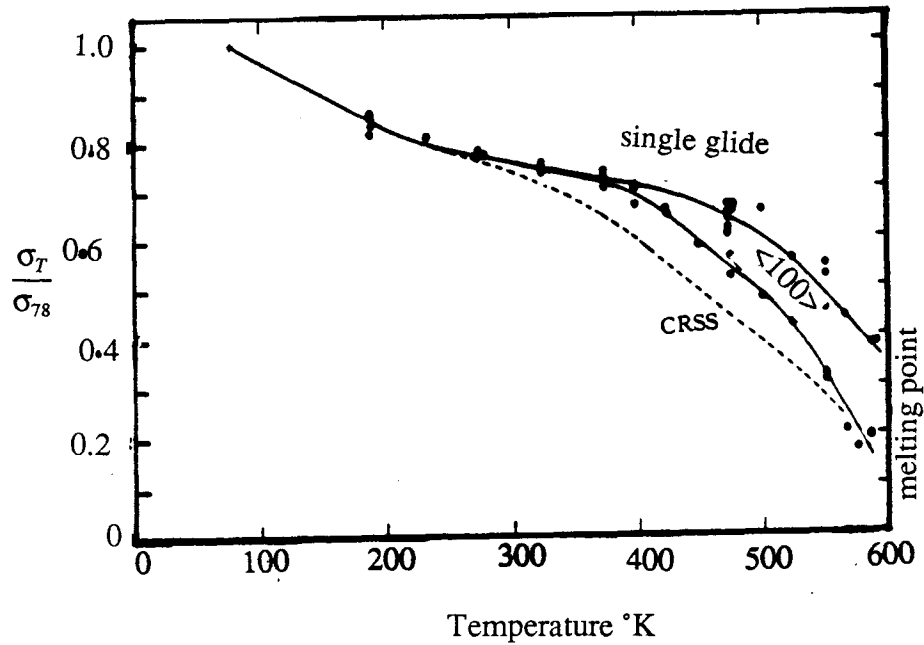


Fig. 1.4(b)

Plastic deformation of lead single crystals as a function of temperature for easy glide and <100> orientations. (a) CRSS (4), (b) flow stress ratio (3).

Above 300°K, it is shown that the CRSS of <100> oriented crystals is effectively the same as easy glide. The flow stress ratio for lead crystals oriented for easy glide is shown in Fig. 1.4(b). The flow stress drops with increasing temperature above 300°K. With <100> orientations, the flow stress above 300°K is a little lower for easy glide as shown in the figure.

The theories of deformation of f.c.c. single crystals generally divides the deformation into three stages. After elastic strain has occurred, stage I of plastic deformation, called easy glide occurs. This is characterised by a very low rate of work hardening and is associated with the occurrence of single slip across the entire cross section of the sample. At high homologous temperatures, stage I is generally not observed.

Following stage I, deformation continues into stage II. In this stage, slip occurs on the primary and secondary slip systems. This stage is one of strong strain hardening with a hardening coefficient that is about ten times that of stage I. The ratio of the work - hardening coefficient to the shear modulus of the material is essentially independent of temperature and the applied stress and is weakly dependent on the specimen orientation. The ratio is insensitive to the impurities present in the material and is of the same order of magnitude for all f.c.c. metals. The linearity of the stress - strain curve in stage II is explained by assuming that the formation of Cottrell- Lomer barriers continues throughout this stage which leads to a decrease in the slip distance with increasing strain. The duration of stage II is temperature dependent. The temperature dependence arises because the yield stress in general increases with decreasing temperature. Consequently the stress necessary for the activation of secondary slip systems also increases as the temperature decreases. At low temperatures, most of the stress - strain curve is dominated by stage II while at high temperatures, it may not be fully developed before the onset of stage III.

Stage III starts when stage II deviates from linearity with increasing strain in the stress - strain curve. In stage III the work hardening coefficient decreases with increasing strain due primarily to dynamic recovery occurring during deformation. With increasing test temperatures, the transition strain between stage II and stage III decreases until stage II cannot be identified at the highest temperatures. The dynamic recovery in this stage is associated with the thermally activated rearrangement of the dislocations in the specimen during deformation. This could include cross slip of screw dislocations and the collapse of Cottrell - Lomer dislocations. These processes reduce the internal stress fields and hence the work hardening coefficient. The stress for the beginning of stage III decreases logarithmically with increasing temperature which can be accounted for by the temperature dependence of the activation energy for cross slip which varies inversely with temperature (5).

### **1.3 Dislocations and Macroscopic Deformation Variables.**

The deformation properties of materials having f.c.c. structures follow a regular pattern. Each material exhibits essentially the same characteristics and in the same order but only differs in the stress and temperature needed to cause the dislocation reactions which controls the given behaviour. The ultimate goal of a study of deformation behaviour is to correlate the dislocation density in the specimen with easily determined macroscopic deformation variables. For GaAs, the dislocation density is determined by chemically etching the sample to produce dislocation etch pits. On {100} surfaces, the etch pits appear as elongated hexagonal shapes. The dislocation density in as grown LEC GaAs crystals is between  $10^4$  to  $10^5$  dislocations / $\text{cm}^2$ . The pits often are arrayed in clusters forming cell boundaries. The dislocation densities are higher at the center and near the edge of a {100} wafer, and in  $\langle 110 \rangle$  directions on the surface. The grown in dislocations have been shown to be highly stable by Gallagher and Weinberg (6), with no apparent movement up to annealing temperatures of  $900^\circ\text{C}$ . They also showed a direct correlation between the etch pits and dislocations using cathodoluminescence imaging of the dislocations.

## 2

**LITERATURE REVIEW**

Dislocations in GaAs have a marked effect on the properties of GaAs devices. It has been shown that n- type Ge can be made p- type by deforming the crystal plastically and the application of an external stress alone is sufficient to cause diode degradation (1). The decrease in light output of GaAs lasers has been related to the kinetic properties of dislocations in the GaAs which are considered to be non - radiative recombination centers. Most of the dislocations in GaAs which affect its electrical and optical properties are produced during crystal growth. As a result a study of the generation and multiplication of dislocations during crystal growth could lead to better control of the density and distribution of the dislocations in GaAs used for devices. In this investigation, the generation and multiplication of dislocations have been examined both experimentally and theoretically.

**2.1 Experimental Study.**

During crystal growth, thermal gradients in the crystal generates local thermoelastic stresses. When the stresses exceed the critical resolved shear stress (CRSS) of the material, dislocations are generated and propagate through the crystal. Attempts to reduce the dislocation density have followed two directions.

1. The thermoelastic stresses can be reduced by reducing the thermal gradients in the crystal. This can be done by changing the thermal environment in the crystal grower by increasing the amount of encapsulant in the liquid or by using a different growth procedure such as Vertical Bridgman growth.
2. Increasing the CRSS of the material by solid solution hardening. It has been reported (7) that adding In dopants to LEC grown GaAs crystals at concentrations up to  $10^{20}/\text{cm}^3$  significantly reduced the dislocation density.

However, although the dislocation density is reduced, the interaction of dislocations with the impurities leads to a range of complex effects in semiconductor devices. Direct measurements of the temperature distributions in the melt and solid during solidification are difficult to make due to the high temperatures involved and particularly the high pressures for GaAs growth. This makes a direct experimental correlation between dislocation density and thermal conditions during growth difficult.

## **2.2 Theoretical Studies.**

Mathematical heat transfer models have been developed to determine the thermoelastic stresses in growing GaAs crystals. Dislocation models have been used to estimate the local dislocation density from the local stresses. Two dislocation models have been considered.

### **2.2.1 The Critical Resolved Shear Stress Model.**

In the plastic deformation of f.c.c. single crystals, the onset of plastic flow is given by the yield stress. For easy glide, with the stress resolved along the slip plane in the slip direction, the onset of plastic flow is given by the critical resolved shear stress (CRSS). The generation and multiplication of dislocations in single crystals occurs when the local stress exceeds the CRSS. The number of dislocations produced increases as the excess local stress increases. For deformation of single crystals at higher temperatures and when more than one slip system is operative, the region of easy glide (stage I) is not observed and the CRSS is thus not clearly defined in the stress strain curve. In addition, the high temperature stress - strain curves have a progressively decreasing slope which makes selection of the yield stress approximate. The application of the CRSS criteria to diamond structure materials has been questioned as well as the effect of temperature on the dislocation density (8). These factors suggest that the CRSS criteria for dislocation generation and multiplication may not be suitable for GaAs.

### 2.2.2 Haasen's Model.

Haasen's model of plastic deformation (2), often referred to as the dynamic dislocation model, is based on the fact that as a material is progressively deformed elastically, part of the strain is progressively relaxed by plastic deformation.

The total strain in the material at any given time is given by the following equation

$$\epsilon_t(t) = \epsilon_p(t) + \epsilon_{el}(t) \quad [1]$$

Where  $\epsilon_t(t)$ ,  $\epsilon_p(t)$ , and  $\epsilon_{el}(t)$  are the total strain, plastic and elastic strains respectively.

The plastic strain rate in the deforming body is given by the Orowan equation

$$\dot{\epsilon}_{pl} = Nbv \quad [2]$$

where  $N$  is the dislocation density,  $b$  the Burgers vector and  $v$  the average dislocation velocity.

Dislocation multiplication occurs in the specimen in proportion to the density of mobile dislocations and the average distance travelled by these dislocations. The multiplication process is defined by

$$dN = \delta N v dt \quad [3]$$

where  $\delta$  is a multiplication parameter assumed to depend on the effective stress since the dislocation velocity depends on the effective stress.  $\delta$  is given by

$$\delta = K \sigma_{eff}^m \quad [4]$$

where the effective stress is by definition given by

$$\sigma_{eff} = \left( \sigma_A - AN^{\frac{1}{2}} \right) \quad [5]$$

K is the multiplication constant,  $\sigma_A$  is the applied stress,  $AN^{1/2}$  is the internal stress at the location of an individual dislocation and m is the stress exponent of the dislocation velocity. In diamond structure materials, m is a small number, with values usually between 1 and 3, and the dislocation velocity is strongly dependent on temperature and weakly dependent on stress (2). In contrast, in f.c.c. metals, m is a large number usually greater than 16, the dislocation velocity is strongly dependent on stress and weakly dependent on temperature (9).

The equation for the dislocation velocity v, is expressed in terms of an Arrhenius type equation since the generation and propagation of dislocations is a thermally activated process as well as being stress activated.

$$v = B(T) (\sigma_A - AN^{1/2})^m \quad [6]$$

where

$$B(T) = B_0 \exp(-U/kT) \quad [7]$$

$B(T)$  is a temperature dependent viscous term describing the changes in the frictional resistance of the lattice to the propagation of dislocations.  $B_0$  is a constant for a given material,  $U$  is the activation energy for the generation of dislocations,  $k$  is the Boltzmann's constant and  $T$  is the test temperature. In contrast, the corresponding equation for the dislocation velocity for f.c.c.metals is given by

$$v = \left( \frac{\sigma_e}{\tau_0} \right)^m \quad [8]$$

$\sigma_e$  is the effective stress on the dislocation,  $\tau_0$  is related to the magnitude of the viscous drag on the moving dislocations by the short range obstacles and  $m$  is the stress velocity exponent. In this model,  $\tau_0$  and  $m$  are considered material constants. In equations [6] and [8], the internal stress is assumed to fluctuate with a wavelength that is of the order of the mean distance between the dislocations. However in equation [8], the assumption is further made that this separation is so large that thermal fluctuations do not assist the applied stress in overcoming the internal stress. This results in a temperature independent flow stress except for the small indirect dependence through the temperature dependence of the elastic constants.

Using equations [1], [2], [3], [4] and [6], the macroscopic stress - strain - time relationship for a deforming specimen is given by a solution of the following simultaneous equations.

$$\frac{dN}{dt} = NK B_0 \exp\left(-\frac{U}{kT}\right) \left(\sigma_A - AN^{\frac{1}{2}}\right)^{m+1} \quad [9]$$

$$\frac{d\varepsilon}{dt} = \phi N b B_0 \exp\left(-\frac{U}{kT}\right) \left(\sigma_A - AN^{\frac{1}{2}}\right)^m + \frac{1}{G} \frac{d\sigma_A}{dt} \quad [10]$$

Where  $\phi$  is a geometrical factor, and  $G$  is the rigidity modulus of the material. The equations are solved subject to the initial conditions that at  $t = 0$ ,  $\varepsilon = 0$  and  $N = N_0$  (where  $N_0$  is the grown - in dislocation density).

### 2.3 The Yield Point.

The model allows the existence of two yield points for the deforming specimen. The upper yield point is defined as the stress at which the initial dislocations present in the specimen begin to move while the lower yield point corresponds to the stress at which the moving dislocations begin to interact with each other (beginning of work hardening). The model accounts for a pronounced yield point in a constant strain rate test using equation [1] as follows. Initially almost all the applied strain is elastic with few dislocations present moving at high speeds. With further deformation the dislocations multiply and the plastic term increases while the elastic term decreases, becomes zero and sometimes negative as the stress goes through the upper yield point. Further dislocation multiplication leads to dislocation interactions which produces a rise in stress resulting in a lower yield point (2).

The temperature and strain rate dependence of the upper and lower yield points can be derived from equations [1], [9] and [10] with the assumption that  $AN^{1/2} \ll \sigma_A$  and is given by

$$\sigma_Y = \left( \frac{A^2 C_m}{b B_0} \right)^{\frac{1}{2+m}} \dot{\epsilon}^{\frac{1}{2+m}} \exp\left( \frac{U}{(2+m)kT} \right) \quad [11]$$

where

$$C_m = \left( 1 + \frac{2}{m} \right)^{2+m} \left( \frac{m}{2} \right)^2 \quad [12]$$

$\sigma_Y$  is the stress at the upper or lower yield point, A and  $C_m$  are constants. The model allows the calculation of the macroscopic deformation variables in terms of the three physical parameters  $B(T)$ , A and K using equations [9] and [10] while equation [11] is used for estimating m and U.

### 2.3.1 Dynamical Recovery.

Haasen's model of plastic deformation has been extended to include the temperature and strain rate dependences of the stress at the beginning of dynamic recovery (15). Using a relation first proposed by Mohamed and Langdon (15), for the description of the steady state creep of materials at high temperatures, the temperature and strain rate dependence of the stress at the beginning of dynamic recovery is given by

$$\frac{\tau_{III}^n}{G} = \frac{AkT}{Gb} \left( \frac{Gb}{\gamma} \right)^3 \dot{\epsilon} \exp\left( \frac{Q_{SD}}{kT} \right) \quad [13]$$

Here,  $n$  is the stress exponent,  $G$  is the shear modulus,  $b$  is the Burgers vector,  $\gamma$  is the stacking fault energy while  $Q_{SD}$  is the activation energy of self diffusion. Equation [13] has been applied to the interpretation of the dynamical recovery of the elemental and compound semiconductors.

## **2.4 Application of Haasen's Model.**

Haasen's model has been used extensively to predict stress - strain curves , creep curves and dislocation densities and to estimate values of  $m$  and  $U$  for the elemental semi- conductors Si and Ge (10,11,12). Because of the close similarity between the crystal structure and electronic bonding of the elemental and compound semiconductors having the sphalerite structure, the model has been successfully applied to GaAs, InSb, InP, and ZnS to estimate  $m$  and  $U$ . (13-24). However the use of equations [9] and [10] to predict the stress - strain curve and dislocation density for GaAs is limited because values of the parameters  $A$ ,  $B(T)$  and  $K$  are not known. The model assumes that all the dislocations in the specimen undergoing deformation are mobile. This assumption limits the application of the model to small strains. Also the model assumes implicitly that the dependence of the dislocation velocity on stress and temperature is separable.

The different values of  $U$  and  $m$  reported when the model was applied at different temperatures and strain rates to the same material were attributed to experimental errors and to the different experimental techniques used in those studies (2,10,12). Weiss (25), while investigating the inflection point of creep curves of germanium observed a temperature dependent stress exponent  $m(T)$  and a stress dependent activation energy  $U(\sigma)$ . He modified Haasen's model to take this into account by replacing the stress exponent in equation [6] by a temperature dependent term given by

$$m(T) = m_0 + \frac{U}{kT} \quad [14]$$

His results are shown in Fig. 2.1 as dashed lines in which the stress associated with the yield point determined from the modified model is plotted as a function of  $\frac{1}{T}$ . Schroter, Brion, and Siethoff (25), in their study of the temperature and strain rate dependence of the lower yield point in silicon and germanium extended the temperature range investigated by Weiss. They deformed silicon and germanium in compression in the temperature range 900°C to 1300°C and 450°C to 920°C respectively and strain rates  $10^{-2}/s$  to  $10^{-5}/s$ . They report that for silicon, the stress exponent of the dislocation velocity ( $m$ ), and the activation energy for the generation of dislocations ( $U$ ), are independent of temperature and applied stress respectively in agreement with Haasen's model. However their results for germanium are in reasonable agreement with the results of Weiss and are shown in Fig. 2.1 by the solid lines.

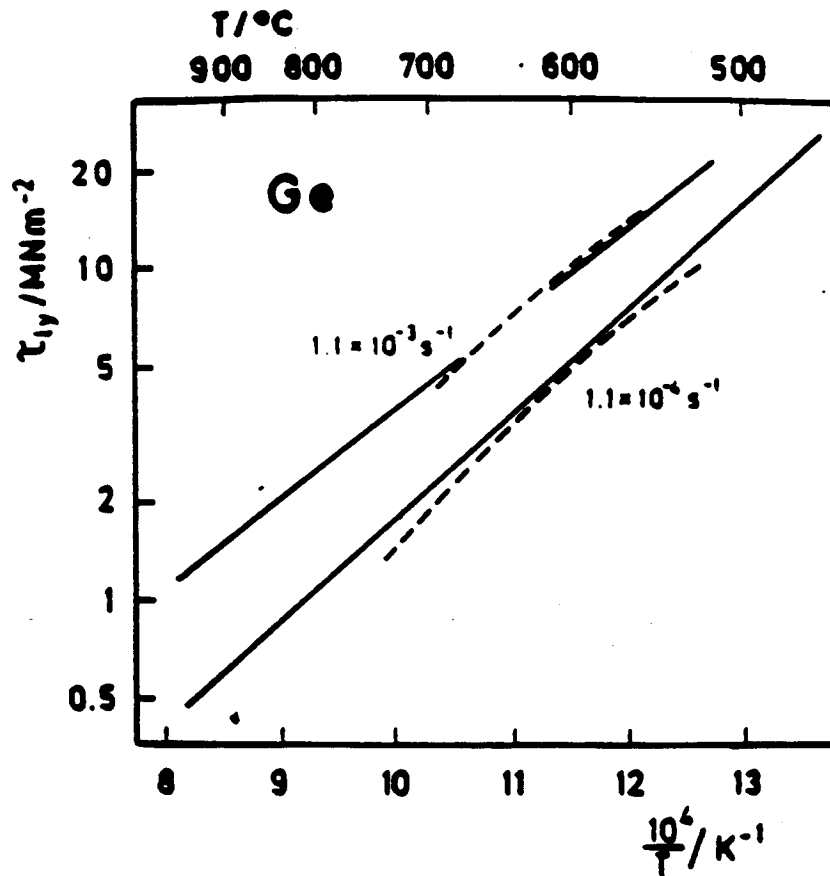


Fig 2.1 Yield stress vs temperature derived from inflection points in creep curves of germanium (dotted lines) at the strain rates indicated (25). The results of Schroter et al for the lower yield point in germanium are indicated by the solid lines (25).

The non linear dotted lines of Weiss differ by a small amount from the solid curves of Schroter et al. There is no clear explanation for this difference and also the different result obtained for silicon. Deformation studies on GaAs have been reported (13,15,16,18) which were carried out in the temperature range of  $350^{\circ}\text{C}$  to  $600^{\circ}\text{C}$ . The temperature and stress dependence of  $m$  and  $U$  were not determined in these investigations.

The ability of Haasen's model to predict the dislocation density in a specimen undergoing plastic deformation is limited because separate experiments are required to estimate  $B(T)$ ,  $A$  and  $K$  in the equation for dislocation density. The density of mobile dislocations in f.c.c. metals can be estimated from a model of plastic deformation by Alden (9,26) which has been compared to experimental data at low temperatures with considerable success. However dislocations in real crystals have been shown to have a fine structure closely related to the crystal structure (27). For GaAs, there are two interpenetrating sublattices of Ga and As forming the f.c.c. structure which gives rise to two types of densely packed glide planes which are not equivalent. In addition, the covalent bonding of GaAs results in a high concentration of energy in the dislocation core and a pronounced Peierl's potential. On the basis of the significant differences between GaAs and f.c.c. metals, it is unlikely that the Alden's model is applicable to GaAs.

### 3

#### OBJECTIVES

The objectives of this research was to extend the range of temperatures generally studied (usually less than 600°C) in the uniaxial plastic deformation of GaAs using compression and tension tests and thus determine

- (a) The temperature and strain rate dependence of the yield stress.
- (b) The activation parameters characterizing the beginning of plastic deformation and observe their temperature and strain rate dependence. With this data, the validity of Haasen's model for the deformation of GaAs will be tested over an extended range of temperature.
- (c) To obtain the dislocation densities in the deformed samples by etching the samples and counting the etch pits. Using these results, the dislocation density will be correlated with the macroscopic deformation variables.

## 4

**EXPERIMENTAL PROCEDURE**

The gallium arsenide single crystals used in the investigation were provided by Johnson Matthey Co Ltd. They consisted of two sets of seed crystals having square cross sections of 36.0mm<sup>2</sup> (series A) and 17.64mm<sup>2</sup> (series B) respectively and wafers of GaAs crystals produced by the LEC method.

**4.1 Determination of The Specimen Orientation.**

The specimen orientations were determined using the Laue back reflection technique. Samples cut from the tensile and compressive specimens were polished and attached to a vertical specimen holder. X-rays were generated at a copper target using a Phillips X-ray machine. The x-ray beam was passed through a 0.5mm diameter pinhole and impinged on the sample positioned 3cm from a flat photographic film placed normal to the incident x-rays and between the x-ray source and the sample. The exposure time was 20minutes at 30kV and 10mA. A fiducial mark made on the film related it's orientation with respect to the sample. A typical x-ray diffraction pattern is shown in Fig. 4.1.

The spots are observed to have four fold symmetry. The normals to the reflecting planes were plotted on a stereographic projection using a stereographic net and a Greninger chart. By comparing the stereographic projection with a standard projection, the spots were identified and the orientation of the sample surface was established as {100}.

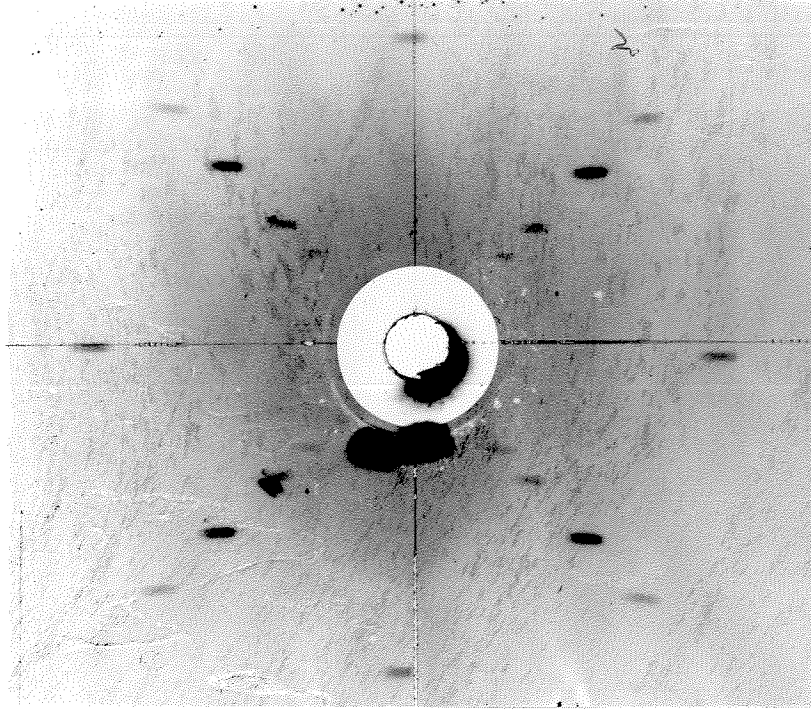


Fig. 4.1 Typical x-ray diffraction pattern obtained in the specimen orientation tests.

## **4.2 Specimen Preparation and Testing.**

### **4.2.1 Compression Tests Specimens.**

A paste of Valtron AD 1210 ingot mounting adhesive was formed by mixing the resin and hardener in the ratio 10 : 1 . Using the paste , the seed crystals were glued to a graphite board one at a time and allowed to dry for about 10 hours. The assembly of the sample on the graphite board was subsequently mounted horizontally on a diamond saw cutting machine. The cutting speed of the diamond blade was set at 2000rpm and the dimensions of the compression specimens were specified on the machine. By operating the cutting machine in the automatic mode, specimens having the set dimensions were cut through a vertical motion of the diamond saw head. After each cutting process, the machine causes the horizontal base which supports the graphite board to move towards the diamond saw head a horizontal distance equal to the set dimensions and the cutting process is repeated. The dimensions of specimens in series A were 6.0mm x 6.0mm x 10mm, and the dimensions of series B were 4.2mm X 4.2mm x 15.9mm. The specimens were separated from the graphite board and the adhesive by heating in a solution of glacial acetic acid. The hot acid weakens the adhesive thus releasing the specimen. The specimens were subsequently polished using a solution of 5 vol % bromine in methanol.

### **4.2.2 Compression Testing Apparatus.**

The apparatus used for the compression tests is shown in Fig. 4.2. It consists of a stainless steel cage into which the test sample is placed as shown. The compression jig is attached to long steel rods which connects it to the load cell and cross head on an Instron machine.

The furnace temperature was measured using a chromel -alumel thermocouple soldered to the test jig beside the specimen. The specimen was heated using a resistance tube furnace and the furnace temperature was recorded on a chart recorder. All tests were conducted in the presence of a helium atmosphere.

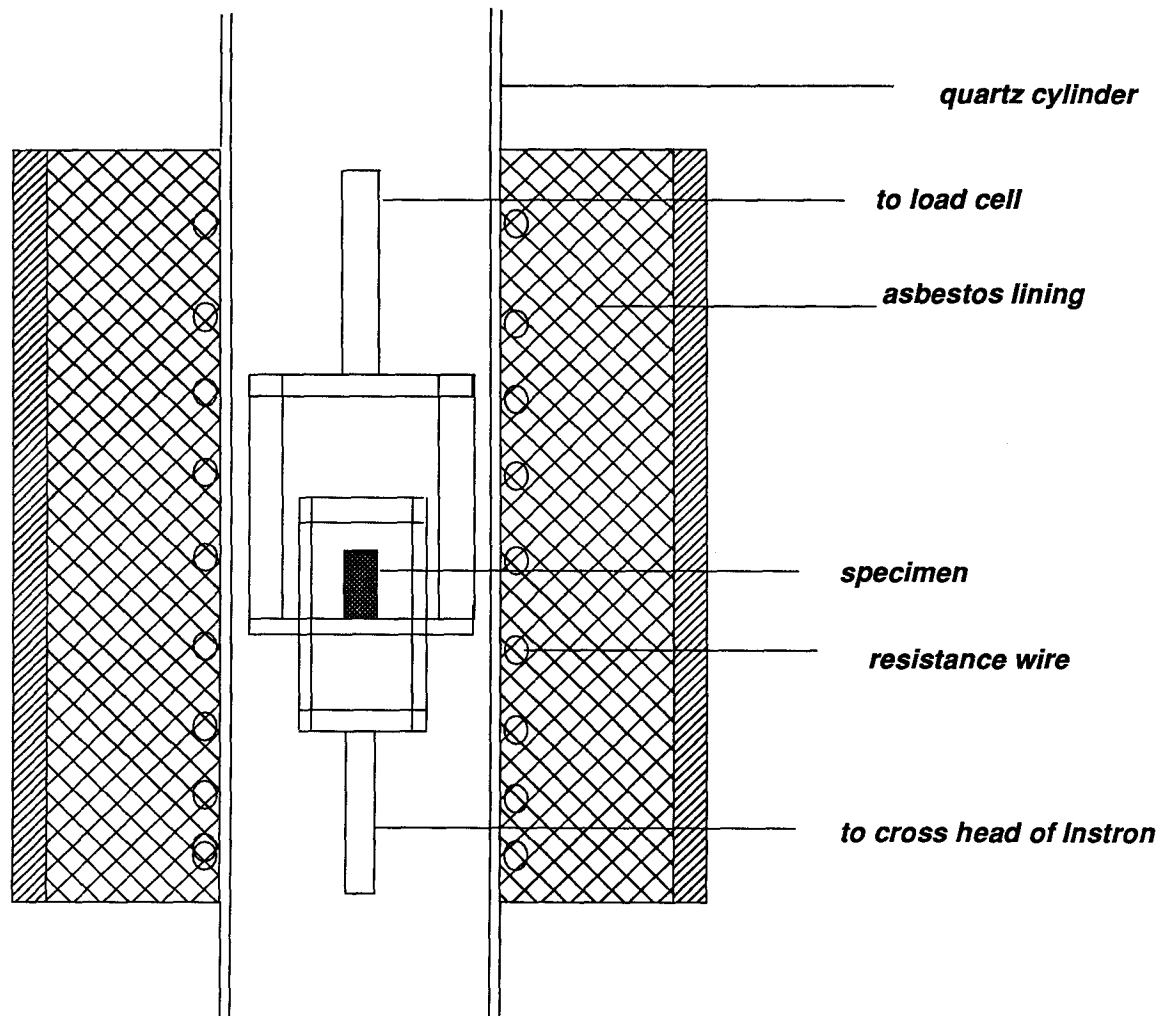


Fig 4.2 Section of the tube furnace enclosing the compression jig.

### 4.2.3 Compression Testing Procedure.

Before each test, the Instron machine was calibrated using a dead weight followed by the calibration of the chart recorder using a voltage generator. The specimen was then placed between the two faces of the compression jig lubricated with graphite, with the deformation axis of the sample parallel to  $\langle 100 \rangle$ . The furnace tube was lowered to enclose the compression jig and the specimen. The furnace was turned on and set to the test temperature and the helium gas flow rate set at 35cc/min. When the furnace temperature reached steady state, the specimen was deformed at a constant cross head speed. The temperature range for the compression test extended from 400°C to 800°C while the cross head speeds (CHS) were varied from  $2.12 \times 10^{-3}$  cm/s to  $8.5 \times 10^{-5}$  cm/s. For each test, the deformation was stopped after a limited amount of plastic deformation occurred. After the furnace has cooled to room temperature, the specimen was removed from the test jig and etched in KOH to determine the dislocation density in the specimen. At the end of each test, the set point temperature was compared with the steady state furnace temperature recorded by the chart recorder. The difference between the two temperatures was not greater than  $\pm 3$  degrees Celsius in all the experiments.

## 4.3 Tensile Tests.

### 4.3.1 Preparation of the Tensile Tests Specimens.

The tensile tests samples were cut from 7.62cm diameter wafers with a thickness of 0.8mm to the shape shown in Fig. 4.3(a). The samples were roughly shaped by sand blasting and finished by grinding the edges with a diamond saw. To do this, an aluminum plate sample was made having the same shape as the tensile specimens. This was then used as a template to mark the shape onto a tape fastened to the GaAs wafer. The tape was cut with a razor blade and the residual tape around the test sample shape removed. This was done on both sides of the GaAs wafer. A fine sand blasting jet cut through the wafer around the edge of the tape fastened to the surface roughly outlining the test sample .

The finishing process was carried out using two glass slides ground to have the same dimensions as the tensile specimen. The glass slides were heated on a hot plate and Lakeside resin was melted onto the surface of each glass slide. The sample was placed between the glass slides, forming a sandwich assembly which was cooled to room temperature. The assembly was then mounted vertically on a grinding machine and by a horizontal motion of the assembly, the upper edge was progressively ground using a high speed diamond impregnated grinding wheel. After each pass, the assembly was raised in small vertical steps of 0.5mm and the process continued until a good surface finish was obtained. The process was then repeated on the opposite edge of the sample. In this way, tensile specimens measuring 15mm x 4mm x 0.8mm were produced. After grinding the assembly was heated on a hot plate and the specimen was separated from the glass slides after the wax melted. The wax residue on the specimen was removed using methyl alcohol and the specimen polished in a 5% bromine / methanol solution , swabbing the surface gently during polishing.

### 4.3.2 Tensile Testing Apparatus.

The tensile samples were mounted in the molybdenum tensile testing grips shown in Fig. 4.3(b). Tests were carried out in an Instron with the upper molybdenum rod of the grips attached to the load cell and the lower to the crosshead. The sample and the test grips were contained in a quartz tube which was filled with helium during testing to reduce oxidation of the sample. The quartz tube was surrounded with a resistance heated tube furnace powered through a temperature controller. Chromel/alumel thermocouples were welded to the upper and lower grip assembly and were used to determine the test temperature.

### 4.3.3 Tensile Testing Procedure.

Initial tests showed that the tensile specimens tended to slip from the grips or deform slightly as they were loaded in the furnace and heated prior to testing. To overcome this, a small titanium guide was attached to the grips to prevent lateral movement of one grip with respect to the other. In addition the tensile samples were cemented to the flat grip surfaces using a high temperature cement (ceramabond 571 powder mixed with the liquid). The tensile axis of the samples were parallel to the  $\langle 100 \rangle$  direction.

The sample fastened to the grips was aligned in the Instron. The heating furnace was then lowered to surround the test assembly and turned on. Helium gas flow through the assembly tube was set at 35cc/min. When the furnace temperature reached steady state at the test temperature (between 400 and 750°C), the sample was deformed in tension at a constant cross head speed (CHS) which varied between  $8.5 \times 10^{-3}$  and  $4.2 \times 10^{-5}$  cm/sec. All the test samples were pulled to fracture, recording the load as a function of time. Examination of the samples after each test showed that elongation and hence plastic deformation took place only in the gauge length, defined as the free specimen length between the upper and lower grips. After the test was completed and the test assembly cooled, the fractured sample

sections were fitted together at the fracture surfaces and the total strain in the gauge length measured. The measured strain was then compared to the strain during plastic deformation determined from the cross head movement. The sample sections were then polished and etched to determine the dislocation density in the deformed sample.

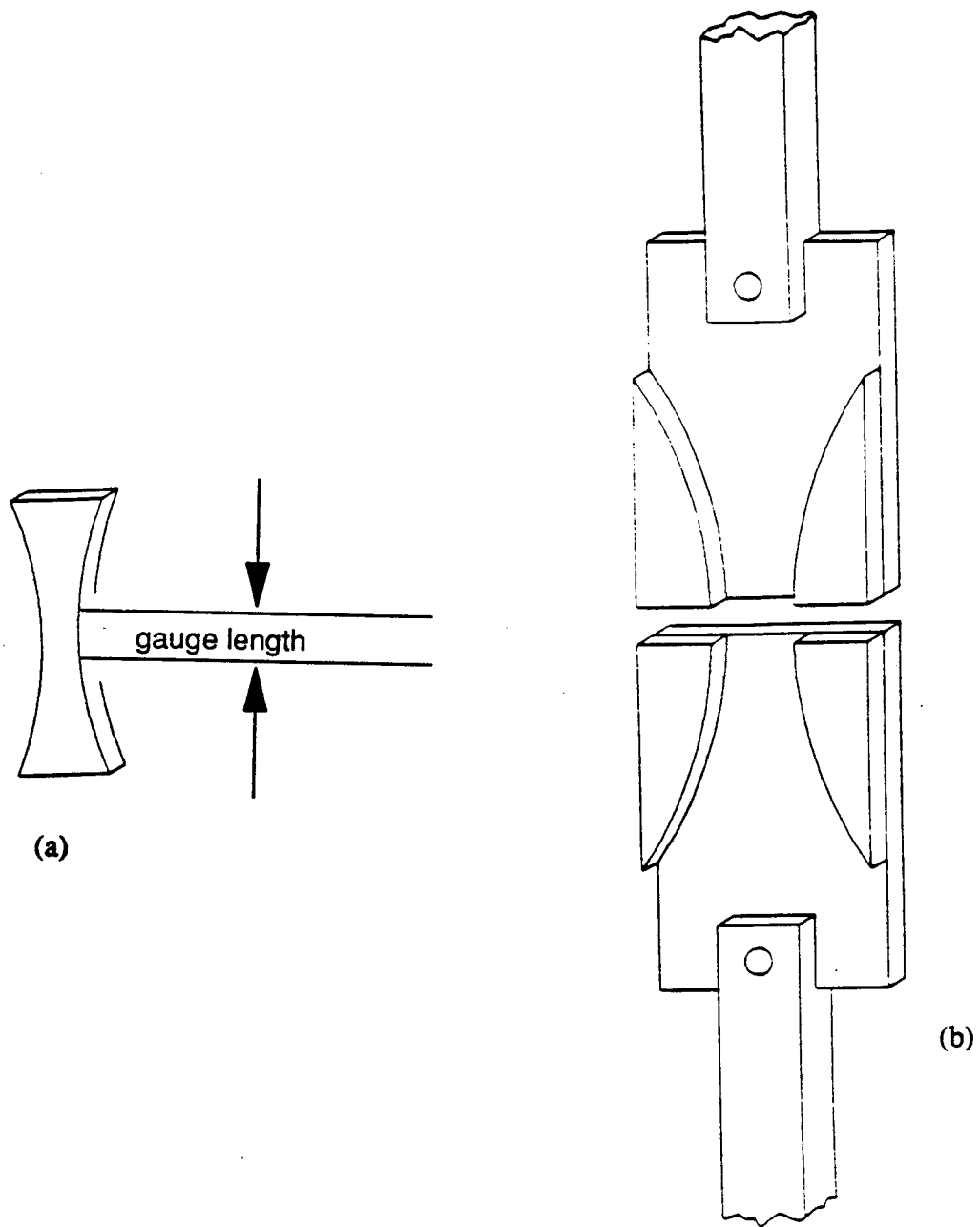


Fig 4.3 (a). Shape of tensile sample, (b) Tensile jig to hold sample.

## **4.4 Dislocation Etch Pit Density.**

Both as received sections of GaAs and sections of test samples after deformation were used for dislocation etch pit density measurements. The samples were initially cleaned by immersing them in boiling trichloroethane, then boiling acetone and finally boiling isopropyl alcohol for five minutes in each liquid. The specimens were then thoroughly washed with distilled water and rinsed with methanol.

### **4.4.1 Chemical Polishing.**

Chemical polishing was carried out in two stages. In the first stage, the specimen was immersed in 15ml of a 1 : 1 : 1 solution of hydrogen peroxide, ammonium hydroxide and distilled water for about three minutes, then washed in distilled water and rinsed in methanol. This removed a thin surface layer of the sample. In the second stage, a solution of 1 : 4 bromine in acetic acid was gently swabbed across the specimen surface using a kimwipe swab until the specimen had a mirror surface. The specimen was then washed with distilled water and rinsed with methanol.

#### **4.4.2 Etching of the Specimens.**

The GaAs specimens were etched one at a time in a nickel crucible. The sample at room temperature was covered with a layer of KOH pellets, a nickel cover placed on the crucible and the crucible placed in a muffle furnace set at 530°C. The crucible was left in the furnace for times ranging from 8 to 12 minutes depending on the specimen size. In the furnace, the potassium hydroxide melted and etched the crystals.

After the specified etching time, the crucible was removed from the furnace and cooled to room temperature. After cooling, the potassium hydroxide was washed off the specimen using running water and the specimen dried with methanol. The etched specimen was then examined for etch pits using an optical microscope at various magnifications.

## 5

### OBSERVATIONS

Haasen's model of plastic deformation relates microscopic dislocation properties to macroscopic deformation variables. Recently the validity of the model for some materials over an extended range of temperature has been questioned. This research was undertaken to test the validity of Haasen's model for GaAs. The model was tested by applying equation [11] to the compression test results. The results of the compression and tension tests also allowed a comparison of the magnitudes of the temperature and strain rate dependence of the yield stresses for the GaAs wafers and the seed crystals. The distribution and density of dislocations in the deformed specimens were also observed.

#### 5.1 Compression Tests Results.

##### 5.1.1 Stress - Strain Curves.

Typical stress - compressive strain curves at 600°C and 700°C test temperatures are shown in Fig. 5.1. The stress and compressive strain were determined from the load and crosshead movement data and the initial dimensions of the sample. The curves show a short initial transition region which varied between samples, followed by a linear section and then a section with progressively decreasing slope as the strain increased. As expected, the curve at 600°C lies above the 700°C curve. Deviation from linearity is gradual and occurs at a higher stress for the 600°C curve as compared to that for 700°C.

On the basis of the plastic strain which occurred in the samples as a result of deformation, determined after completion of the test, elastic deformation occurred in the initial transient. The linear section is taken as stage II during plastic deformation and the

section with decreasing slope as stage III. Since the samples have  $\langle 100 \rangle$  parallel to the deformation axis, in which case multiple slip systems are operative, stage I should not be observed in the stress strain curve.

The resolved shear stress - shear compressive strain curves were derived from the stress - strain curves using.

$$S = \sigma \cos \lambda \cos \phi \quad [15]$$

where  $S$  is the resolved shear stress while  $\cos \lambda \cos \phi$  is the Schmid factor. The samples were oriented with the (100) plane in the compression plane. Slip occurred on the {111} planes in  $\langle 110 \rangle$  directions. The angle  $\lambda$ , between the normal to the {111} and the compression direction is  $54^\circ 44''$  and that between the  $\langle 110 \rangle$  direction and the compression axis  $\phi$ , is  $45^\circ$ . Accordingly the Schmid factor is 0.409. The resolved shear stress is the measured stress times the Schmid's factor while the resolved shear strain is the measured compressive strain times the reciprocal of the Schmid's factor.

Examples of the resolved shear stress - resolved shear strain curves for series B compression tests samples between  $500^\circ\text{C}$  and  $800^\circ\text{C}$  test temperatures are shown in Fig. 5.2. The linear stage II is observed to shorten rapidly with increasing test temperature, followed by a curved portion with progressively decreasing slope. The slope of stage II decreases with increasing test temperature. The transition from the linear stage II to non-linear stage III of the stress strain curves is not clearly defined. The transition point is taken as the intersection of two straight lines, one drawn along the linear portion and the other drawn tangent to the curved portion as shown in Fig. 5.3. This is termed the recovery stress which is the resolved shear stress at the start of dynamical recovery. The yield stresses and

the stresses at the beginning of dynamical recovery determined as a function of temperature and strain rates are listed for series A samples in Table 5.1 while that of series B samples are listed in Tables 5.2 (a) and (b). In Table 5.1, we note that the yield stress drops from 10.08 MPa at 400°C to 3.02 MPa at 750°C for a CHS of  $4.2 \times 10^{-4}$  cm/s. Increasing the CHS to  $8.5 \times 10^{-4}$  cm/s increases the yield stress at 500°C to 9.58 MPa. The yield stress values for the B samples (Table 5.2(a)) with the larger length/width ratio vary between 7.55 MPa at 400°C and 3.47 MPa at 800°C for a CHS  $4.2 \times 10^{-4}$  cm/s. The yield stress increases at higher values of CHS and decreases with lower values. Comparing the results in Tables 5.1 and 5.2 (a), it is noted that the yield stress values are significantly lower for the B series compared to the A series.

The difference between the A and B series is attributed to the lower length/width ratio of the A series. It has been shown (28), that below a length/width ratio of about 2.0, end effects significantly raise the apparent yield stress. Series A specimens has a length/width ratio of 1.67 which is below the critical value while series B specimens has a length/width ratio of 3.8. The temperature dependence of the yield stress of the series B samples for the three strain rates examined are shown in Fig. 5.5. Highest values of yield stress are obtained for the highest strain rate. At 500°C, the yield stress corresponding to strain rate of  $0.333 \times 10^{-4}$ /s is appreciably lower than the others.

Each sample after deformation was measured and the change in length due to deformation compared to the change in length determined from the Instron chart recording the load and elongation during deformation. The results for series B samples are listed in Table 5.3. The measured change in length  $\Delta l$  is observed to be lower than the value determined from the Instron chart by 4 to 29 %.

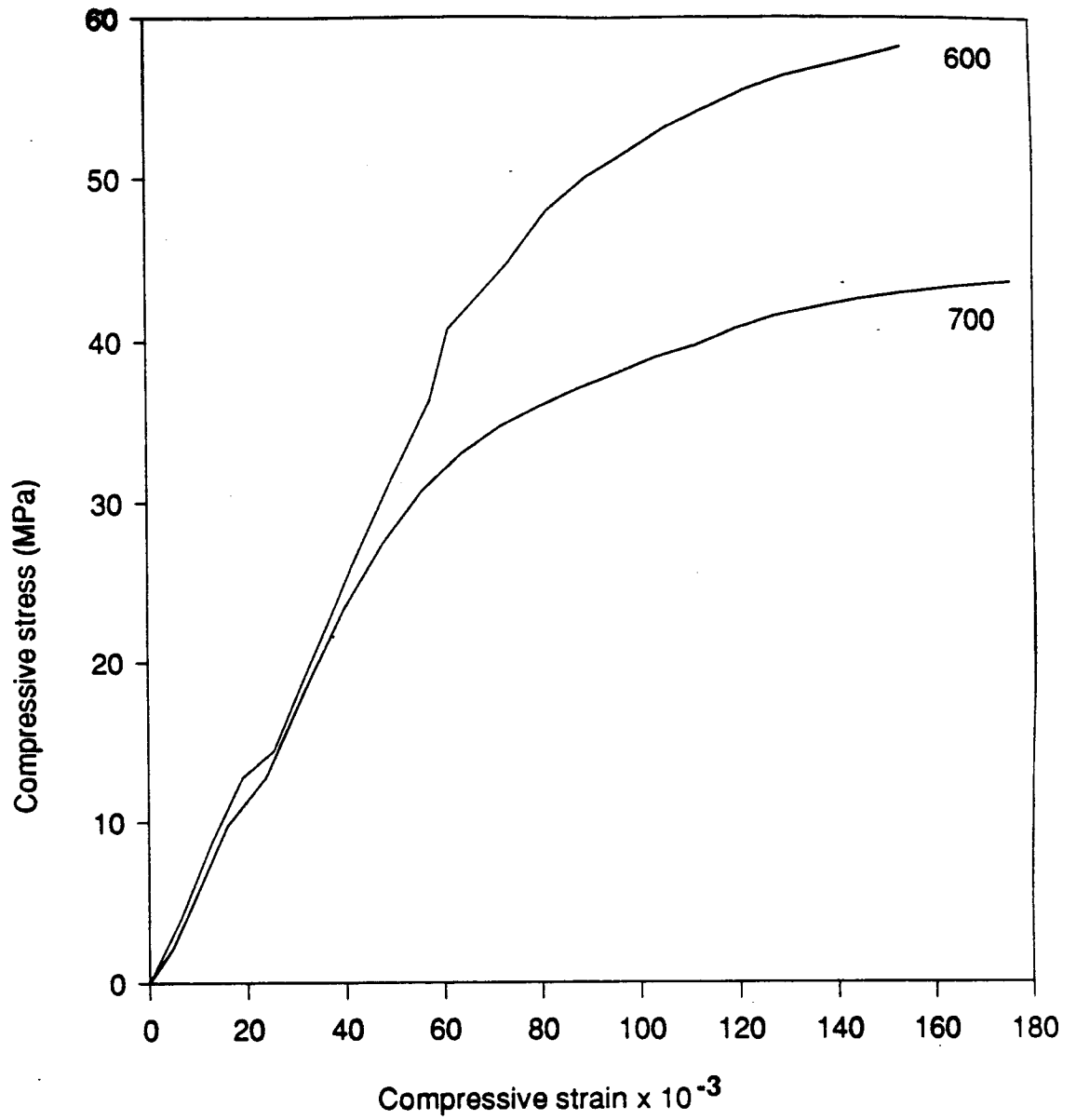


Fig. 5.1 Typical stress - compressive strain curves obtained in the compression tests for the test temperatures indicated and a CHS of  $4.2 \times 10^{-4}$  cm/sec. (Sample numbers 7B and 10B).

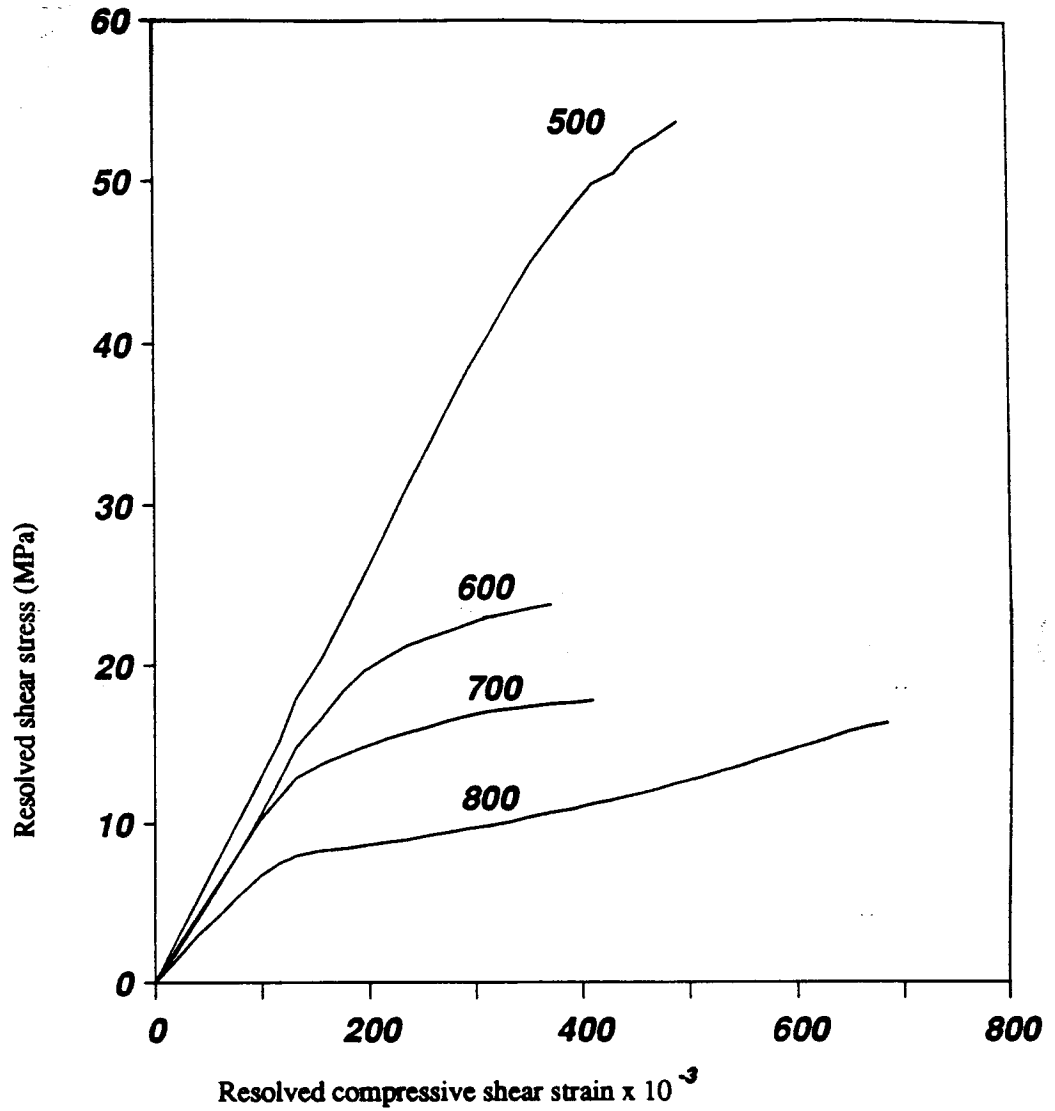


Fig. 5.2 Resolved shear stress - Shear compressive strain curves for the test temperatures indicated °C and a CHS of  $4.2 \times 10^{-4}$  cm/sec. (Sample numbers 4B, 7B, 10B and 13B).

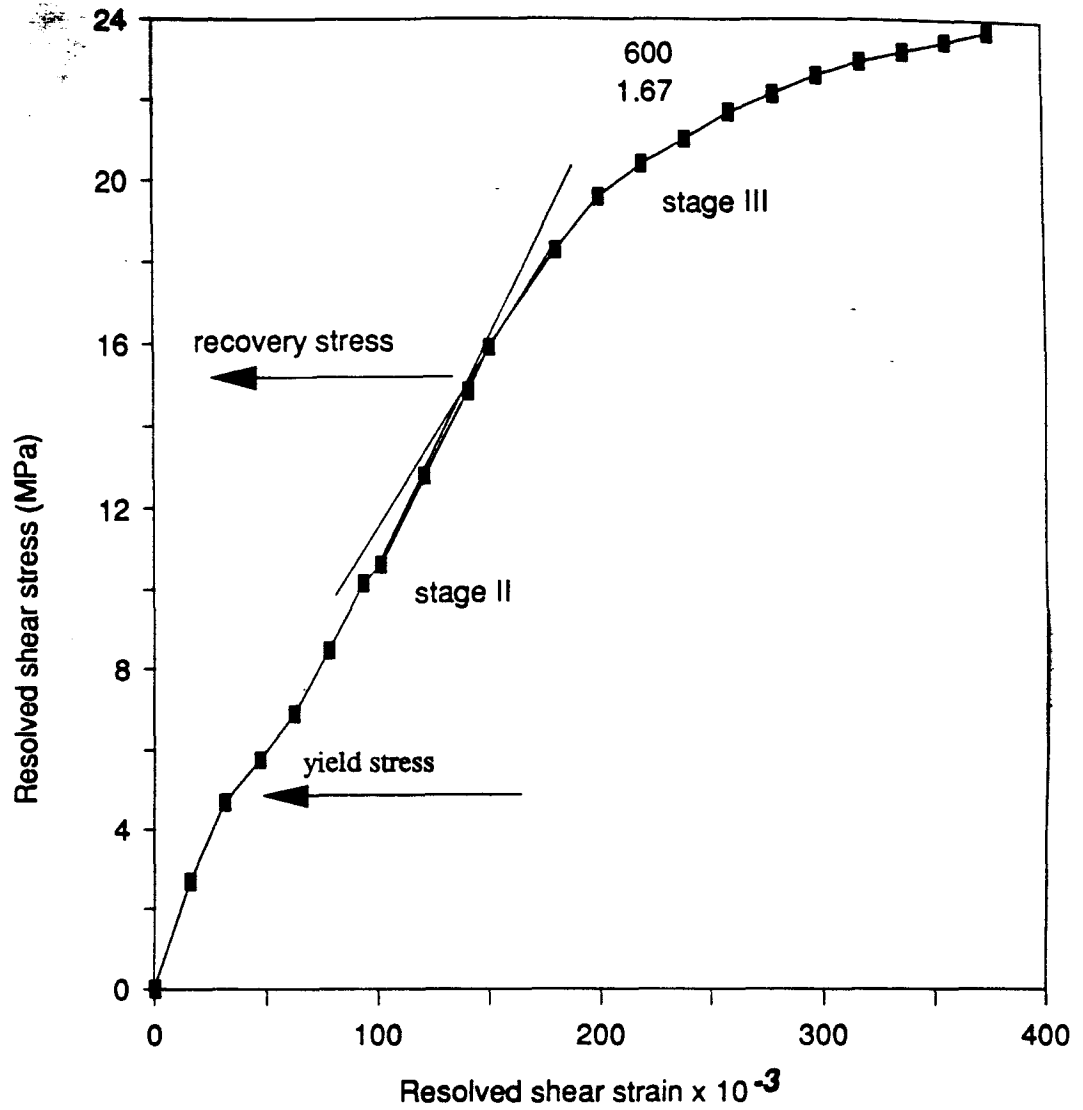


Fig. 5.3 Determination of the recovery stress from the resolved shear stress - shear strain curves for the temperature and strain rate indicated (Sample number 7B).

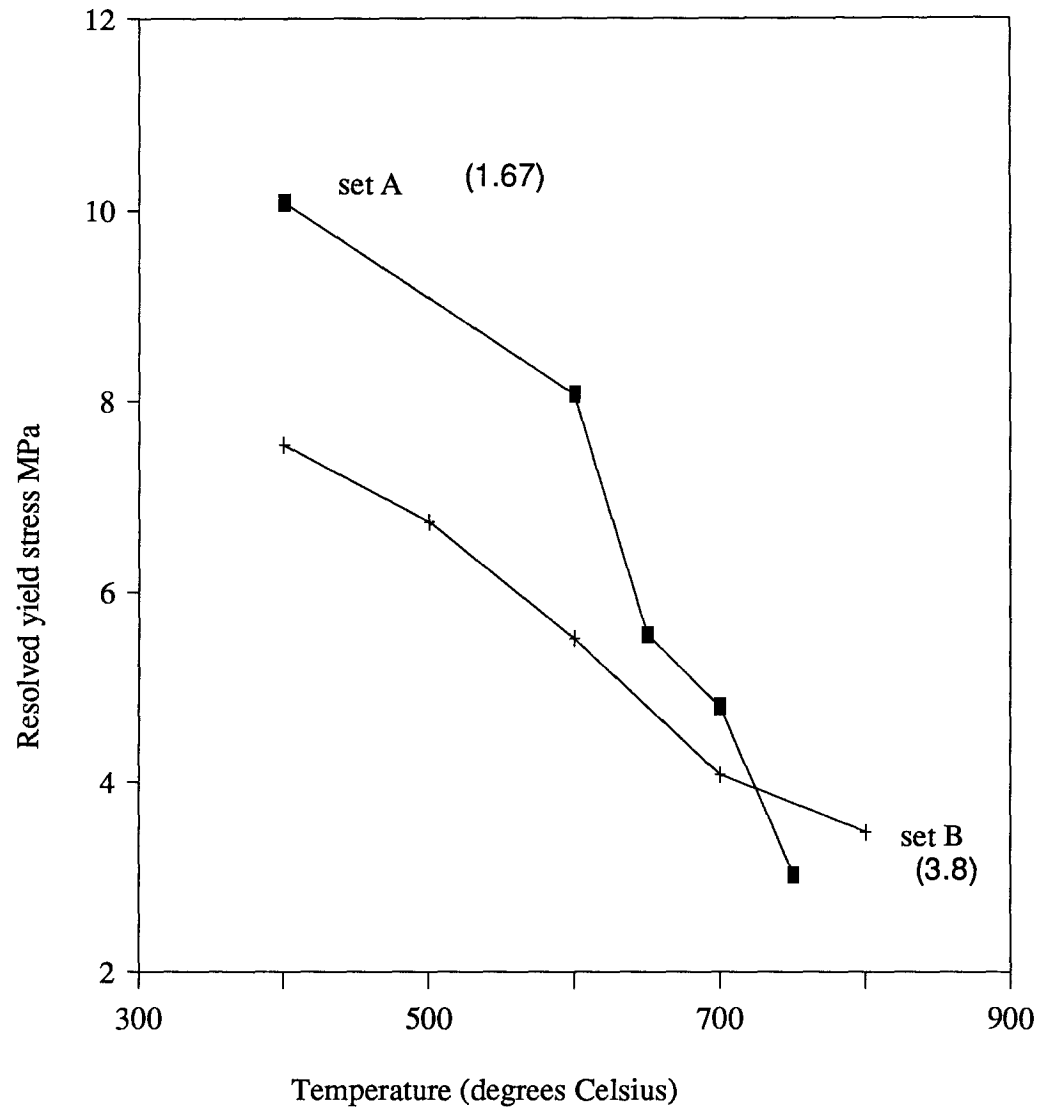


Fig. 5.4 Comparison of the yield stress against temperature for the two sets of compression tests specimens for the length/width ratios indicated. (CHS =  $4.2 \times 10^{-4}$  cm/s).

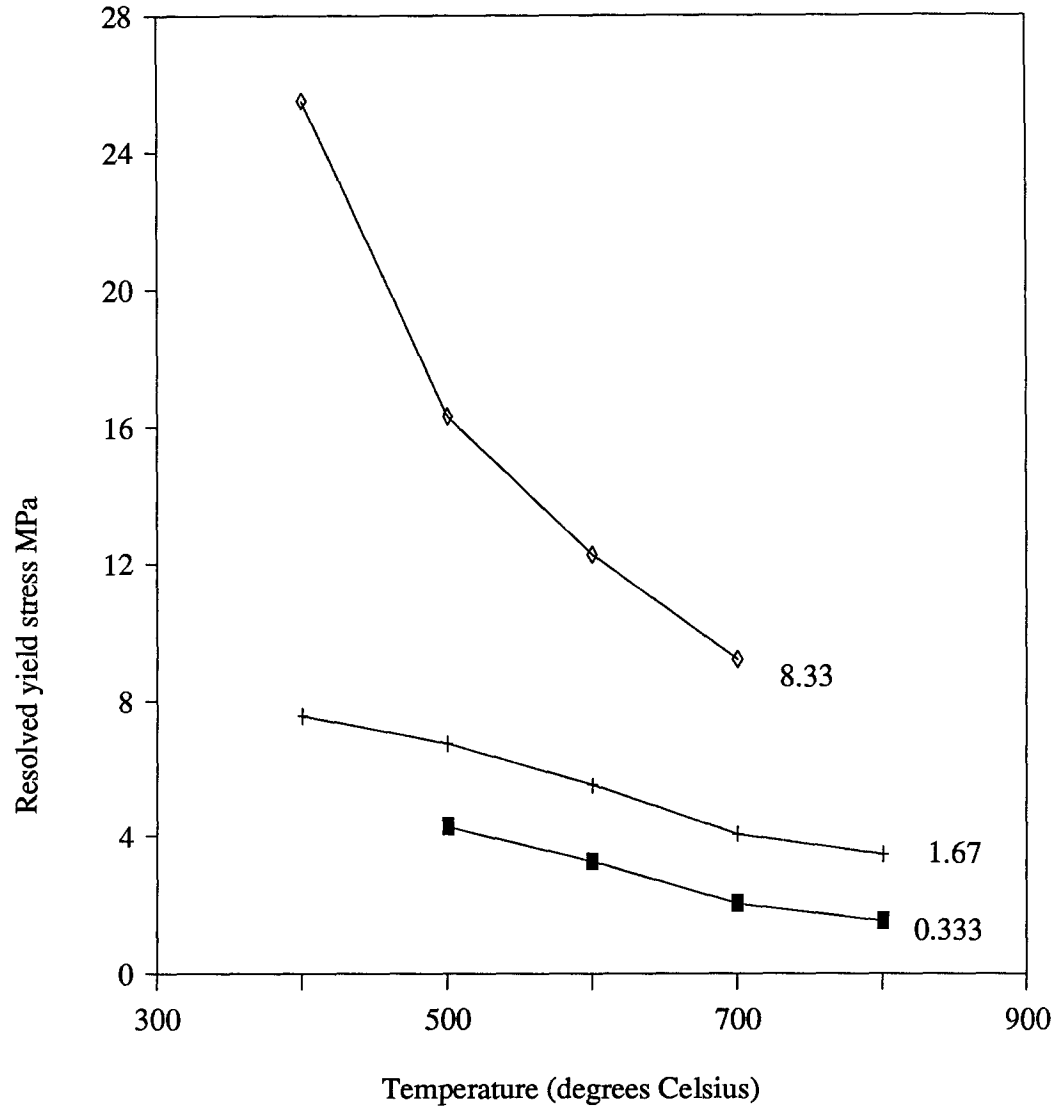


Fig. 5.5 Temperature dependence of the yield stress for the strain rates indicated (  $\times 10^{-4}$  /sec), for the series B compression tests specimens.

Temperature °C	Sample	Yield Stress (MPa)	$\tau_{III}$ (MPa)	Strain Rate x $10^{-4}$ /s	CHS (cm/sec) x $10^{-4}$
400	1A	10.08	48.52	1.67	4.2
500	2A	9.58	52.42	3.33	8.5
600	3A	8.07	29.23	1.67	4.2
650	4A	5.55	27.47	1.67	4.2
700	5A	4.79	17.89	1.67	4.2
750	6A	3.02	15.12	1.67	4.2

Table 5.1 Temperature dependence of the yield stress and the recovery stress for the series A compression tests specimens (Sample dimensions 6.0 x 6.0 x 10.0mm).

Temperature °C	Sample	Yield stress ( $\sigma_Y$ ) (MPa)	$\ln \sigma_Y$	Strain Rate x $10^{-4}/s$	CHS (cm/sec)
400	1B	25.52	17.05	8.33	$2.1 \times 10^{-3}$
400	2B	7.55	15.84	1.67	$4.2 \times 10^{-4}$
500	3B	4.29	15.27	0.33	$8.5 \times 10^{-5}$
	4B	6.74	15.72	1.67	$4.2 \times 10^{-4}$
	5B	16.33	16.61	8.33	$2.1 \times 10^{-3}$
600	6B	3.27	15.00	0.33	$8.5 \times 10^{-5}$
	7B	5.51	15.52	1.67	$4.2 \times 10^{-4}$
	8B	12.25	16.32	8.33	$2.1 \times 10^{-3}$
700	9B	2.04	14.53	0.33	$8.5 \times 10^{-5}$
	10B	4.08	15.22	1.67	$4.2 \times 10^{-4}$
	11B	9.19	16.03	8.33	$2.1 \times 10^{-3}$
800	12B	1.53	14.24	0.33	$8.5 \times 10^{-5}$
	13B	3.47	15.06	1.67	$4.2 \times 10^{-4}$

Table 5.2(a). Temperature dependence of the yield stress for series B compression tests specimens (Specimen dimensions 4.2 x 4.2 x 15.9mm).

Temperature °C	Sample	$\tau_{III}$ (MPa)	$\ln \tau_{III}$	Strain Rate x $10^{-4}/s$	CHS (cm/sec)
400	1B	50.02	17.72	8.33	$2.1 \times 10^{-3}$
400	2B	43.39	17.59	1.67	$4.2 \times 10^{-4}$
500	3B	17.35	16.67	0.33	$8.5 \times 10^{-5}$
	4B	35.22	17.38	1.67	$4.2 \times 10^{-4}$
	5B	40.83	17.52	8.33	$2.1 \times 10^{-3}$
600	6B	11.84	16.29	0.33	$8.5 \times 10^{-5}$
	7B	15.72	16.57	1.67	$4.2 \times 10^{-4}$
	8B	25.52	17.05	8.33	$2.1 \times 10^{-3}$
700	9B	6.34	15.66	0.33	$8.5 \times 10^{-5}$
	10B	10.41	16.16	1.67	$4.2 \times 10^{-4}$
	11B	13.48	16.42	8.33	$2.1 \times 10^{-3}$
800	12B	3.27	15.00	0.33	$8.5 \times 10^{-5}$
	13B	6.53	15.69	1.67	$4.2 \times 10^{-4}$

Table 5.2(b). Temperature dependence of the recovery stress for series B compression tests specimens (Specimen dimensions 4.2 x 4.2 x 15.9mm).

Temp. °C	Sample	$\Delta l$ (chart) mm	$\Delta l$ (sample) mm	CHS (cm/sec)
400	1B	3.05	2.69	$2.1 \times 10^{-3}$
400	2B	4.83	4.32	$4.2 \times 10^{-4}$
500	3B	4.78	4.06	$8.5 \times 10^{-5}$
	4B	3.25	3.02	$4.2 \times 10^{-4}$
	5B	6.35	5.18	$2.1 \times 10^{-3}$
600	6B	1.63	1.45	$8.5 \times 10^{-5}$
	7B	2.41	2.29	$4.2 \times 10^{-4}$
	8B	5.84	5.61	$2.1 \times 10^{-3}$
700	9B	1.37	0.97	$8.5 \times 10^{-5}$
	10B	2.74	2.51	$4.2 \times 10^{-4}$
	11B	9.40 *	5.89	$2.1 \times 10^{-3}$
800	12B	3.05	2.67	$8.5 \times 10^{-5}$
	13B	4.45	4.14	$4.2 \times 10^{-4}$

Table 5.3 A comparison of sample elongations determined from Instron chart and by a direct measurement of changes in sample length (\* sample fractured).

### 5.1.2 Temperature and Strain Rate Dependence of $m$ and $U$ .

In the previous theoretical consideration of deformation, an expression was developed for the yield stress as a function of the material parameters and the test conditions (equation [11]), and reproduced below

$$\sigma_Y = \left( \frac{A^2 C_m}{b B_0} \right)^{\frac{1}{2+m}} \dot{\epsilon}^{\frac{1}{2+m}} \text{Exp}\left( \frac{U}{(2+m)kT} \right)$$

On taking the natural logarithm of the above equation, we obtain

$$\ln \sigma_Y = \frac{1}{2+m} \ln \left( \frac{A^2 C_m}{b B_0} \right) + \frac{1}{2+m} \ln \dot{\epsilon} + \frac{U}{(2+m)kT} \quad [16]$$

At constant temperature,  $U$  is assumed constant independent of the applied stress, then equation [16] may be written as

$$\ln \sigma_Y = C + \frac{1}{(2+m)} \ln \dot{\epsilon} \quad [17]$$

where

$$C = \frac{1}{2+m} \ln \left( \frac{A^2 C_m}{b B_0} \right) + \frac{U}{(2+m)kT} \quad [18]$$

From equation [17],  $\ln \sigma_Y$  should be linearly dependent on  $\ln \dot{\epsilon}$  with a slope given by  $\frac{1}{(2+m)}$ . Values of  $\ln \sigma_Y$  were plotted as a function of  $\ln \dot{\epsilon}$  in Fig. 5.6 for the compression tests samples (Table 5.2(a)). The solid lines were obtained by a least squares fit of the

experimental results. The magnitude of  $(2+m)$  for any given test temperature is given by the reciprocal of the slope of the fitted line and the results are listed in Table 5.4(a). since the results at 400 and 800°C are only based on two points, the values listed are uncertain.

For a constant strain rate and variable temperature, equation [16] may be written as

$$\ln \sigma_Y = D + \frac{U}{(2+m)kT} \quad [19]$$

where D is a constant given by

$$D = \frac{1}{(2+m)} \left( \ln \left( \frac{A^2 C_m}{b B_0} \right) + \ln \dot{\epsilon} \right) \quad [20]$$

from equation [19],  $\ln \sigma_Y$  should be linearly dependent on  $\frac{1}{T}$  with a slope given by  $\frac{U}{(2+m)k}$  where k is the Boltzman's constant. Values of  $\frac{U}{(2+m)}$  were estimated using

$$\frac{U}{(2+m)} = k \cdot \text{slope} \quad [21]$$

Values of  $\ln \sigma_Y$  are plotted against  $1/T$  for three strain rates in Fig. 5.7, the solid lines being a best fit of the experimental points. From the resulting slopes  $\frac{U}{(2+m)}$  is determined from equation [21], giving values of 0.19, 0.13 and 0.13 eV for the strain rates of 0.33, 1.67 and  $8.33 \times 10^{-4}$  /s respectively.

By a similar analysis using equation [13], the strain rate dependence of the stress at the beginning of dynamic recovery is given by

$$n \ln \tau_{III} = \text{Constant} + \ln \dot{\epsilon} \quad [22]$$

From equation [22],  $\ln \tau_{III}$  should be linearly related to  $\ln \dot{\epsilon}$  with a slope given by  $\frac{1}{n}$ . Values of  $\ln \tau_{III}$  are plotted against  $\ln \dot{\epsilon}$  for the various test temperatures in Fig. 5.8. The solid lines are a least squares fit of the experimental results. The magnitudes of  $n$  are obtained from the reciprocals of the slopes of the curves and are listed in Table 5.5(a).

The temperature dependence of the recovery stress is similarly obtained from equation [13] as

$$n \ln \tau_{III} = \text{Constant} + \frac{Q_{SD}}{kT} \quad [23]$$

Thus  $\ln \tau_{III}$  is linearly related to  $1/T$  with a slope given by.

$$\text{slope} = \frac{Q_{SD}}{nk}$$

$$\therefore \frac{Q_{SD}}{n} = k \cdot \text{slope}$$

Values of  $\ln \tau_{III}$  are plotted against  $1/T$  in Fig. 5.9 for the three strain rates. The solid lines represent a least squares fit of the experimental results. From the resulting slopes,  $\frac{Q_{SD}}{n}$  were estimated and the values are listed in Table 5.5(b).

The present results for  $(2+m)$  are compared with values reported in the literature in Table 5.4(b). It is observed that the present results are a little higher than the reported values for other specimen orientations. This difference may be associated either with the different orientations of the specimens or due to residual strain in the sample. Note that the pre-strained sample listed in Table 5.4(b) has a high value for  $(2+m)$ . Values for  $\frac{U}{(2+m)}$  from the present results are correspondingly lower than the reported values.

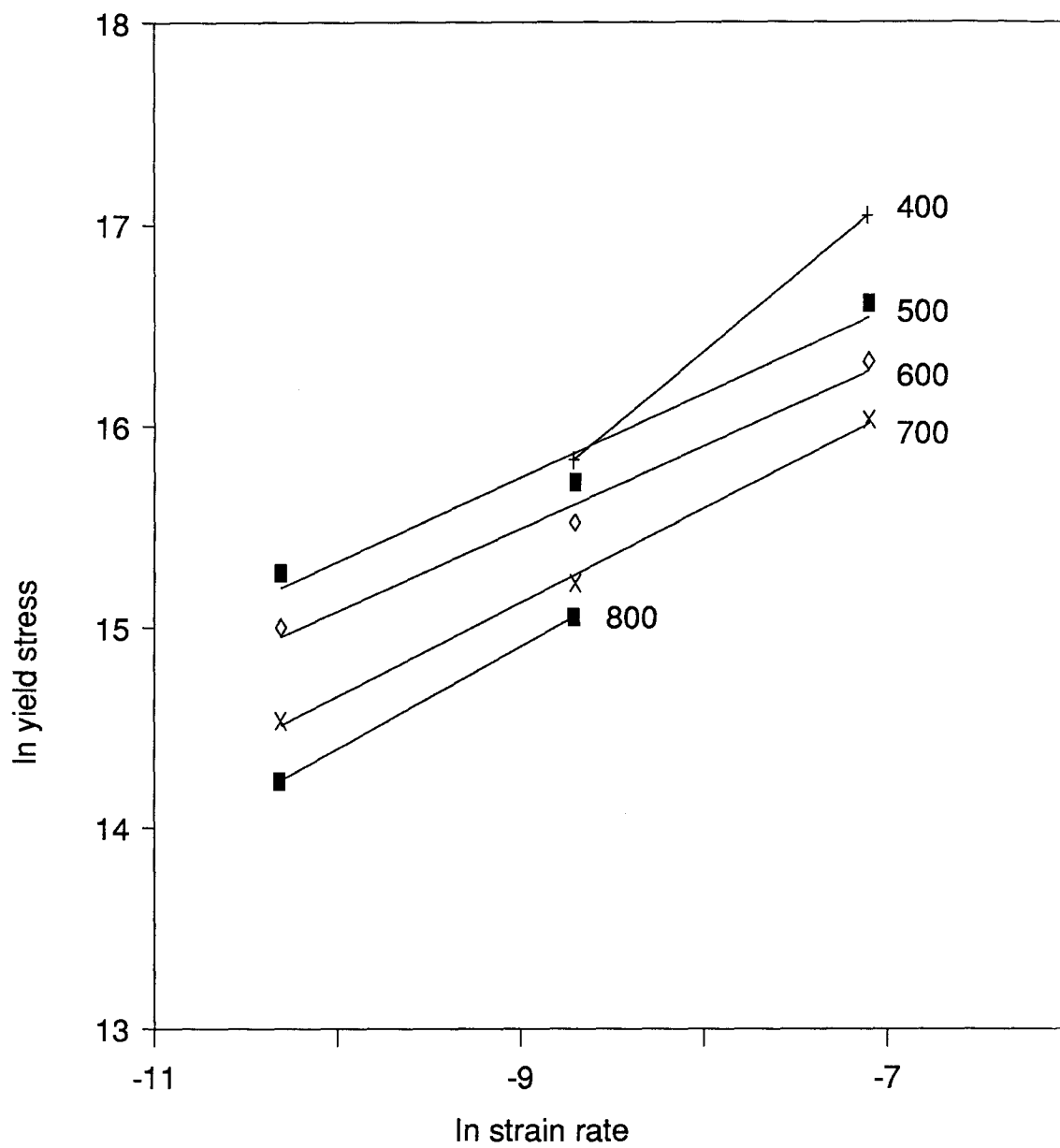


Fig. 5.6  $\ln$  yield stress vs  $\ln$  strain rate for the test temperatures indicated °C.

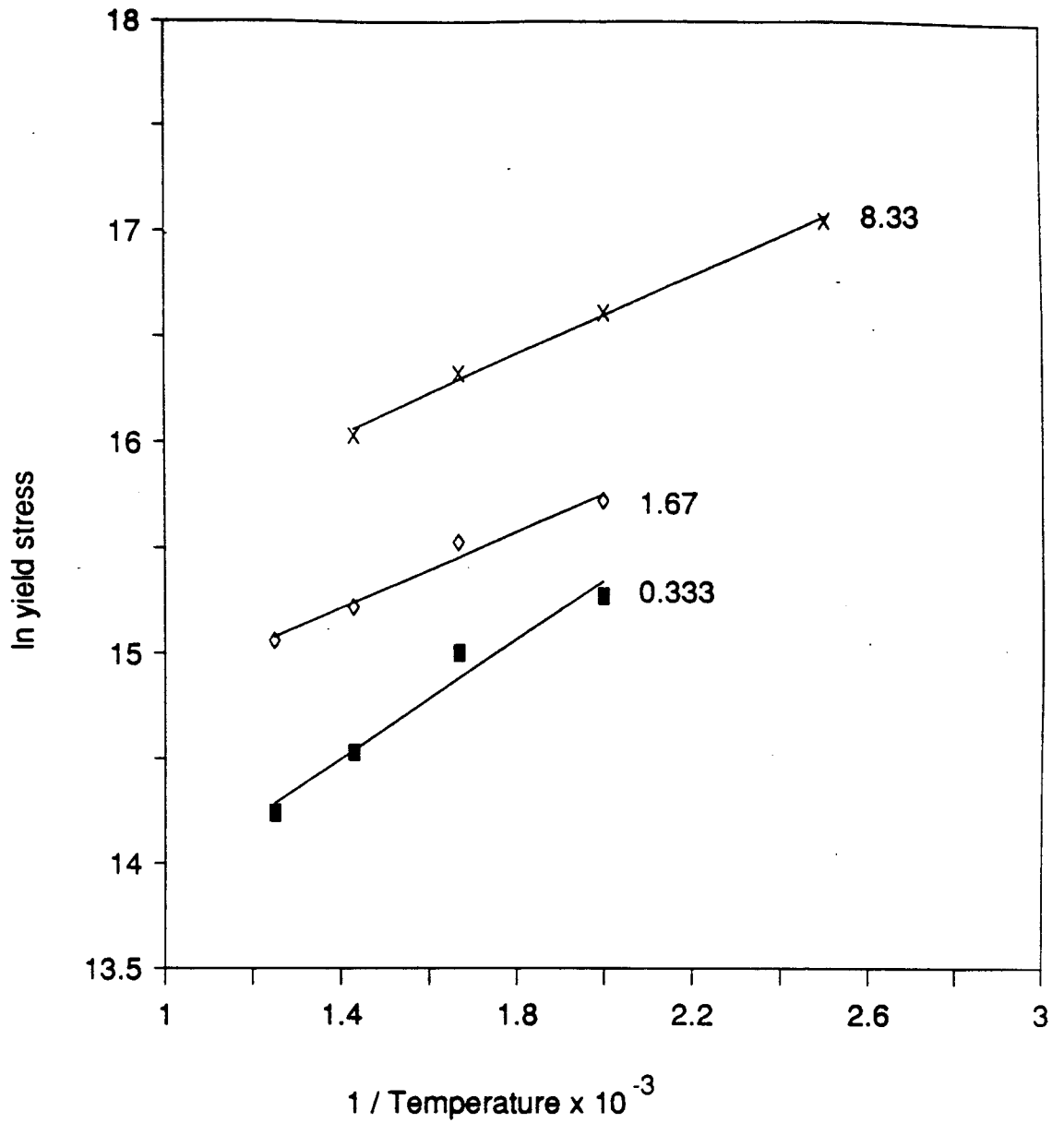


Fig 5.7 ln of the yield stress vs the reciprocal of the test temperature for the strain rates indicated x 10<sup>-4</sup>/s.

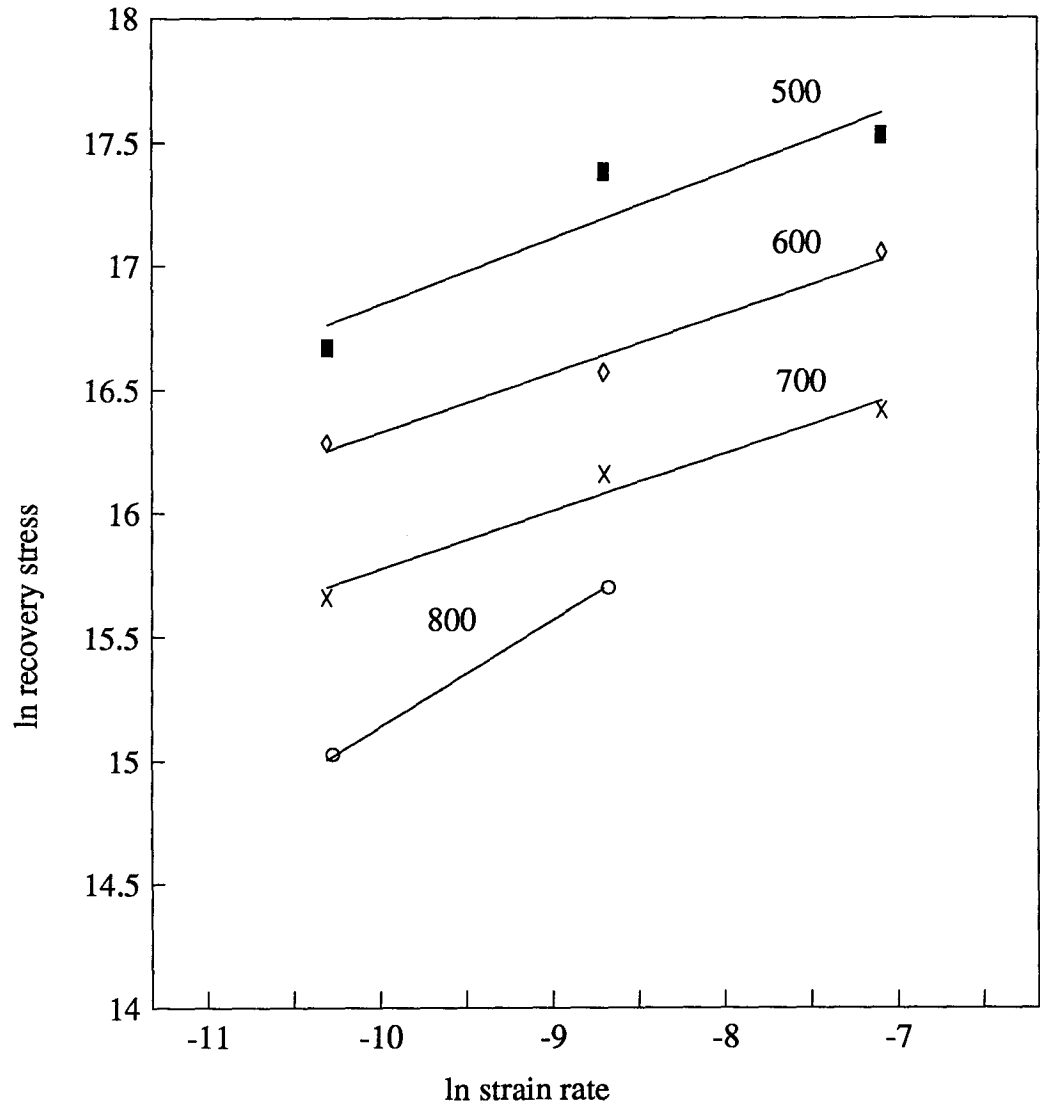


Fig. 5.8 ln of the recovery stress vs ln strain rate for the test temperatures indicated  
°C.

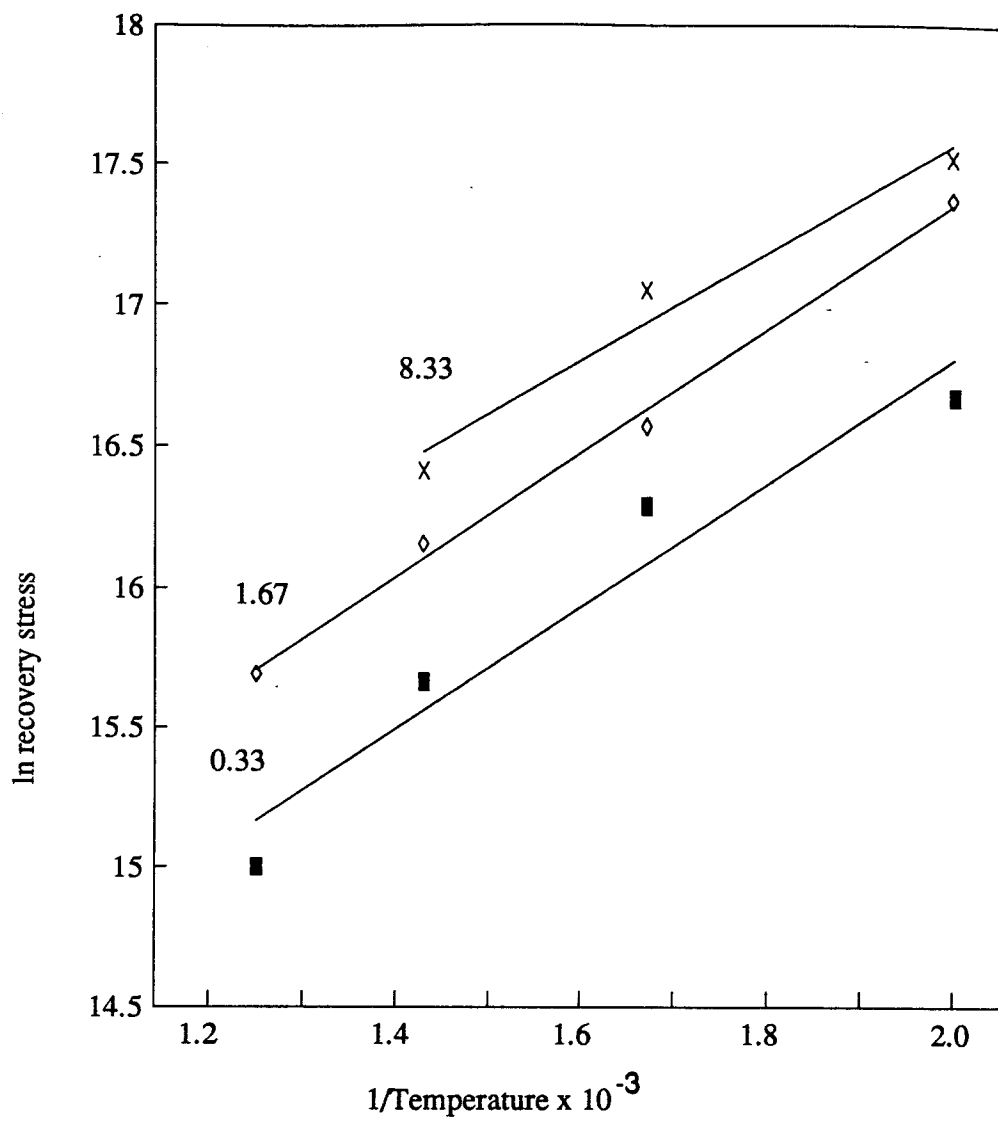


Fig 5.9  $\ln$  of the recovery stress vs the reciprocal of the test temperature for the strain rates indicated  $\times 10^{-4}/\text{s}$ .

Temperature °C)	$\frac{T}{T_m}$	(2+m)
400	0.323	3.33
500	0.404	4.40
600	0.485	4.44
700	0.565	4.15
800	0.646	3.96

5.4(a).

Crystal Orientation	$\frac{T}{T_m}$	$\frac{U}{(2+m)} eV$	(2+m)
<110>	0.41 - 0.58	0.45	3.2
<123>	0.45 - 0.51	0.45	3.1
<123>	0.46 - 0.62	0.35	3.5
<123>	0.35 - 0.58	0.31	6.5*

Table 5.4(b).

Values of (2+m) determined from the present data for <100> oriented crystals (Table 5.4(a)). Reported values of  $U/(2+m)$  and (2+m) for the crystal orientations indicated are listed in Table 5.4(b). The value with the asterisk is for a pre - strained sample (15).

Temperature °C	$\frac{T}{T_m}$	n
500	0.40	3.8
600	0.48	4.2
700	0.57	4.3
800	0.65	2.3

Table 5.5(a)

Strain Rate x 10 <sup>4</sup> /s	$\frac{Q_{SD}}{n}$ eV
0.333	0.19
1.67	0.20
8.33	0.17

Table 5.5(b).

Tables 5.5(a) and 5.5(b) n and  $\frac{Q_{SD}}{n}$  values obtained from the present study.

### 5.1.3 Dislocation Density - Compression Tests

The dislocation density in the undeformed and deformed compression tests samples were obtained by etching the samples and counting the etch pits. An example of the etch pit density and distribution in an as received sample after etching in KOH for eight minutes is shown in Fig. 5.10. The etch pits are clearly defined with hexagonal symmetry. There is a variation in etch pit size and some overlapping of the pits. The etch pit density was counted to be  $4.0 \times 10^4/\text{cm}^2$  which is within the range of the values reported for as grown GaAs crystals.

After deformation, the etch pits were not as clearly defined and had an appreciably higher density than that of the as received sample. An example is shown in Fig. 5.11 for a sample tested at  $600^\circ\text{C}$  at a strain rate of  $8.33 \times 10^{-4}/\text{s}$ . There appears to be two categories of etch pits on the surface. One consists of large elongated faceted pits, and a large number of small black pits. The density of the large pits were counted to be  $1.5 \times 10^5$  pits/ $\text{cm}^2$  which is close to the as received etch pit density. The estimated density of the small pits is  $4.42 \times 10^6$  pits/ $\text{cm}^2$ . These pits may be associated with the dislocations resulting from plastic deformation. The small pits appear to be arrayed in lines which might correspond to slip lines. Another example of a compression sample deformed at  $600^\circ\text{C}$  at a slower strain rate is shown in Fig. 5.12. The etch pit distribution is similar to that of Fig. 5.11 with similar large and small pits but with a slightly higher density. The dislocation etch pit densities in deformed compression tests samples (series B) are listed in Table 5.6.

Temp. °C	Sample	Strain rate $\times 10^{-4} /s$	$\sigma_A - \sigma_Y$ (MPa)	$\epsilon_P$	Calculated etch pit Density $\times 10^6 /cm^2$	Observed etch pit Density (large) $\times 10^5 /cm^2$	Observed etch pit Density (small) $\times 10^6 /cm^2$
						large	small
400	1B	8.33	25.01	0.096	1.88		1.46
500	4B	1.67	40.16	0.172	3.40	9.4	3.58
600	6B	0.333	15.10	0.095	2.89	0.89	4.3
600	8B	8.33	24.58	0.255	4.66	1.5	4.42
700	9B	0.333	10.01	0.047	4.90		4.47
800	12B	0.333	4.90	0.199	6.45		6.12

Table 5.6. Dislocation etch pit density in deformed compression test samples (series B),  $\sigma_A - \sigma_Y$  is the difference between the final stress in the sample and the yield stress,  $\epsilon_P$  is the plastic strain in the sample.

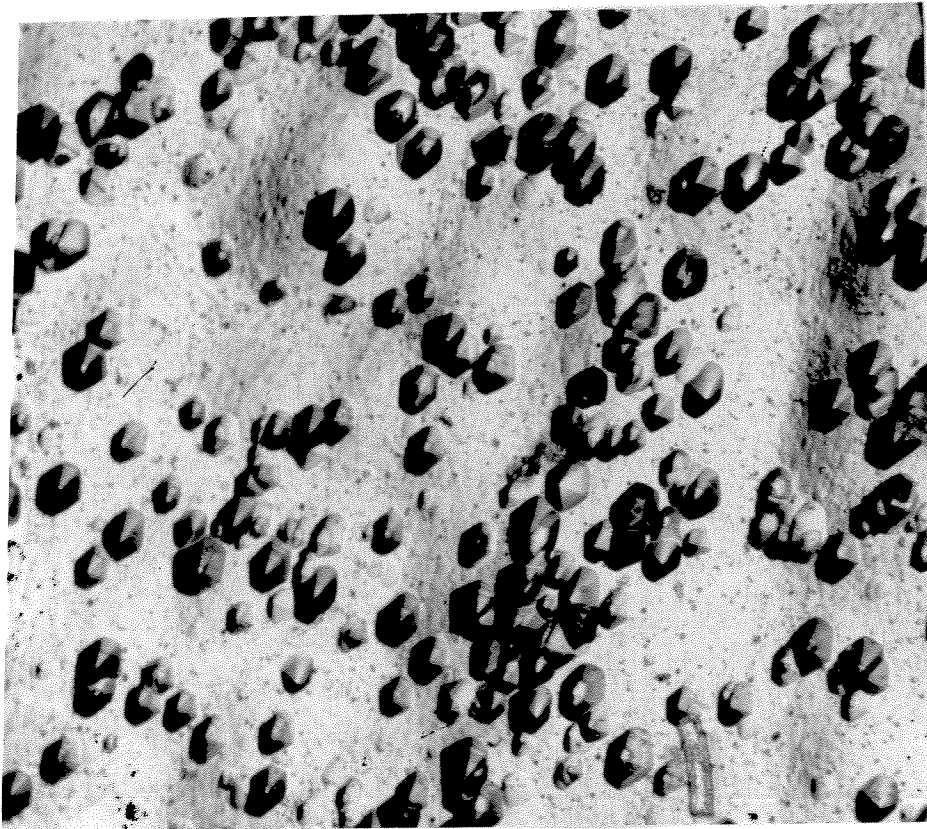


Fig 5.10 Dislocation etch pits in an as received GaAs sample (set B). Etching time was 8 minutes. Magnification X 175.

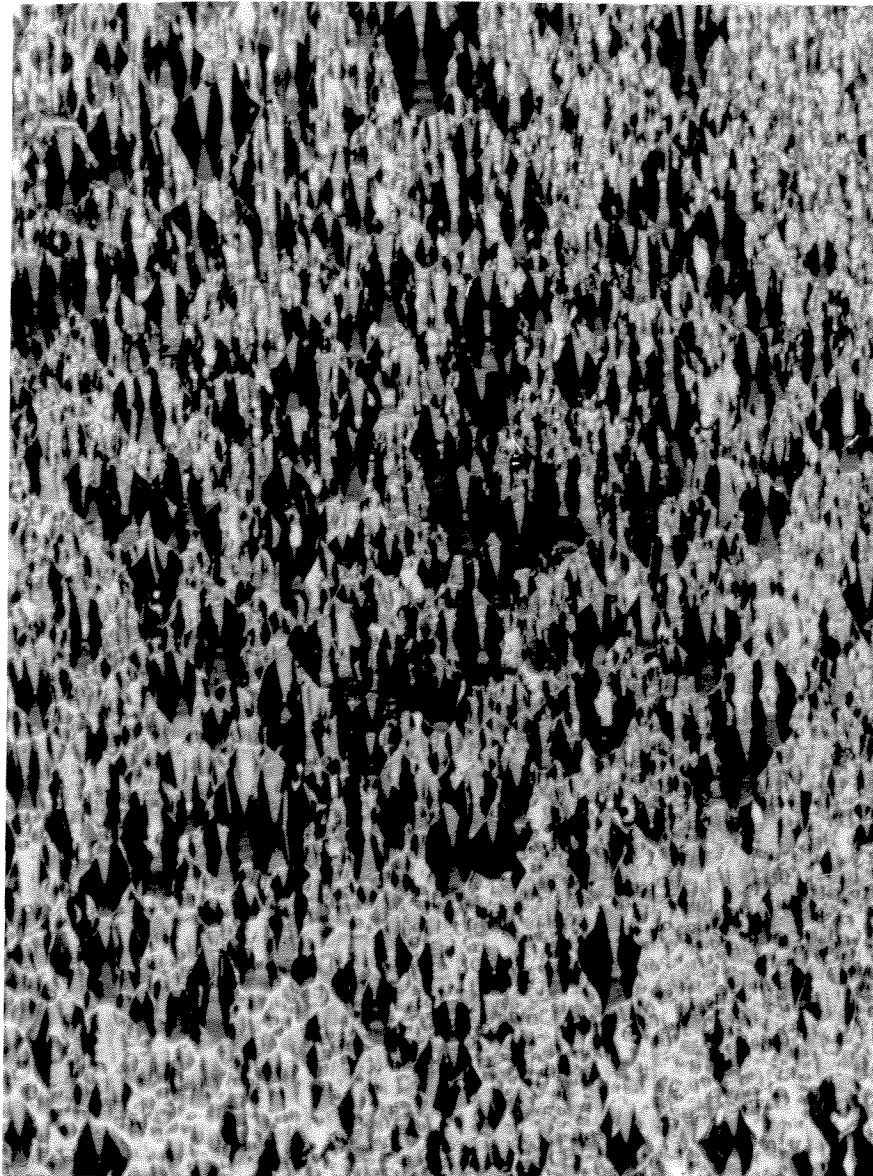


Fig 5.11 Dislocation etch pits in a deformed GaAs sample (strain rate =  $8.33 \times 10^{-4}$ /s, test temperature =  $600^{\circ}\text{C}$ ). Magnification X 600, Specimen number 8B.

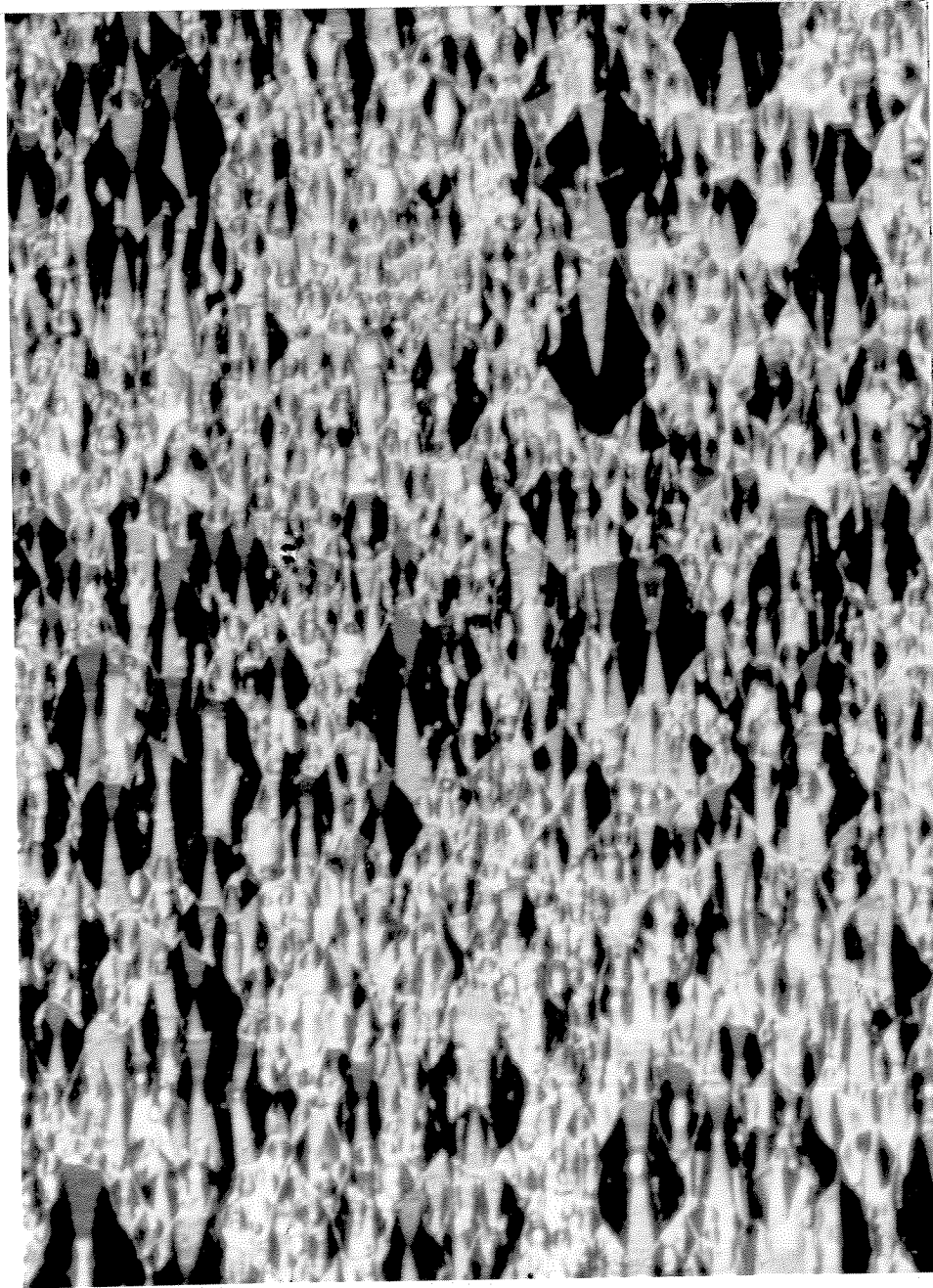


Fig 5.12 Dislocation etch pits in a deformed GaAs sample. (strain rate =  $3.33 \times 10^{-5}$  /s, test temperature =  $600^{\circ}\text{C}$ .) Magnification X 950, Specimen number 6B.

## **5.2 Tensile Tests.**

### **5.2.1 Tensile Stress - Tensile Strain Curves.**

A typical stress - strain curve for GaAs at 700°C strained at  $1.67 \times 10^{-4}$ /s is shown in Fig. 5.13. The curve show a linear stage II followed by a non - linear stage III with a progressively decreasing slope. All the samples fractured at the end of the deformation without any apparent necking. The plastic strain at fracture as a function of temperature in samples which deformed plastically is shown in Fig. 5.14. The data available is limited. However the results show that considerable plastic deformation occurred prior to fracture. Up to 93 % plastic strains were observed depending on the test temperature and strain rate.

### **5.2.2 The Temperature Dependence of The Yield Stress.**

The values of yield stresses obtained in the present study are shown in Table 5.7. The temperature dependence of the yield stresses for the two strain rates considered is shown in Fig. 5.15. The yield stress for the higher strain rate is significantly above the corresponding values for the lower strain rate. The recovery stress was obtained from the stress - strain curves in a manner similar to that shown in Fig. 5.3 and the results obtained in the present study are shown in Table 5.7.

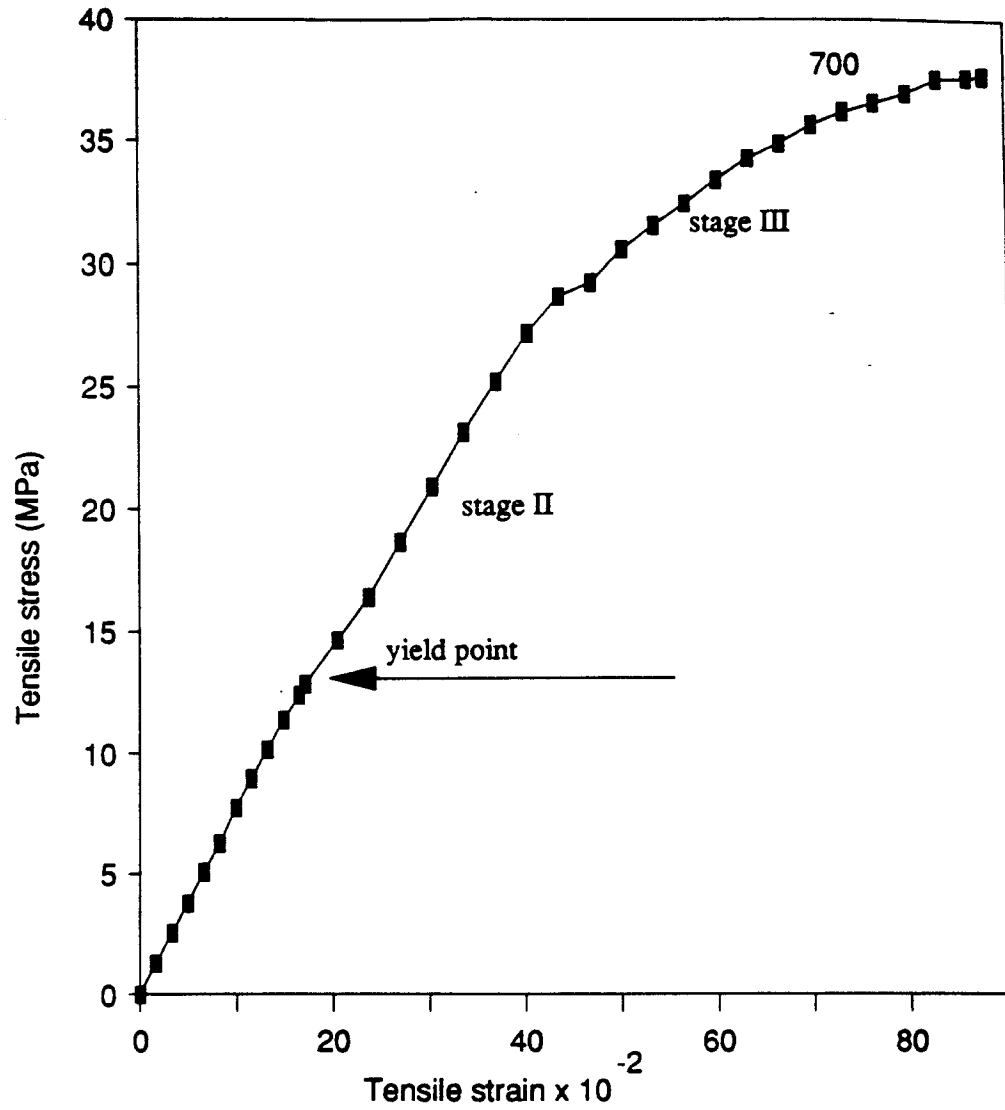


Fig. 5.13 Typical stress - strain curve obtained in tension tests for the test temperature indicated °C and a strain rate of  $1.67 \times 10^{-4}$ /s (sample number T12).

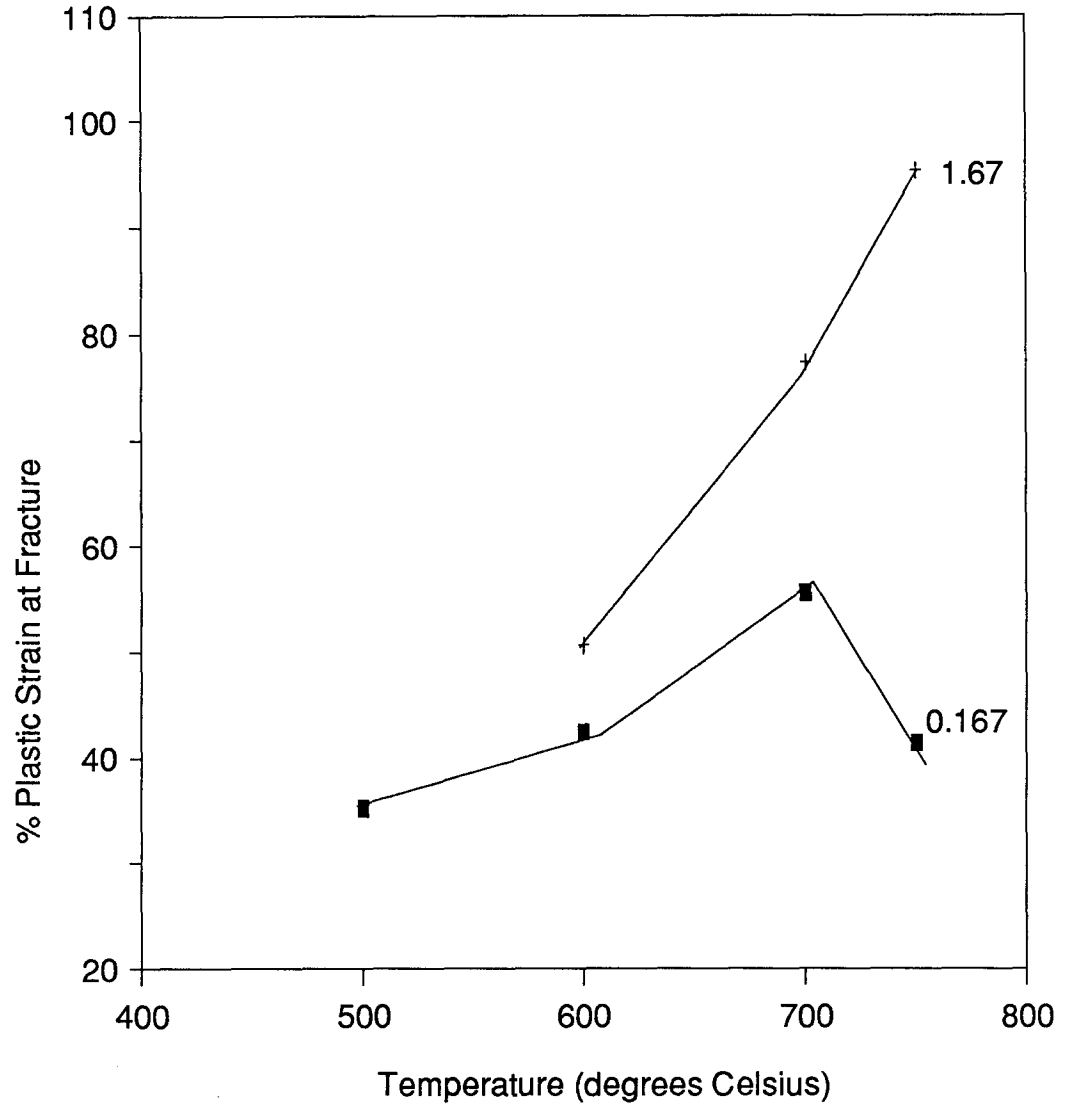


Fig 5.14 The percentage plastic strain at fracture as a function of test temperature for the strain rates indicated  $\times 10^{-4}/s$ .

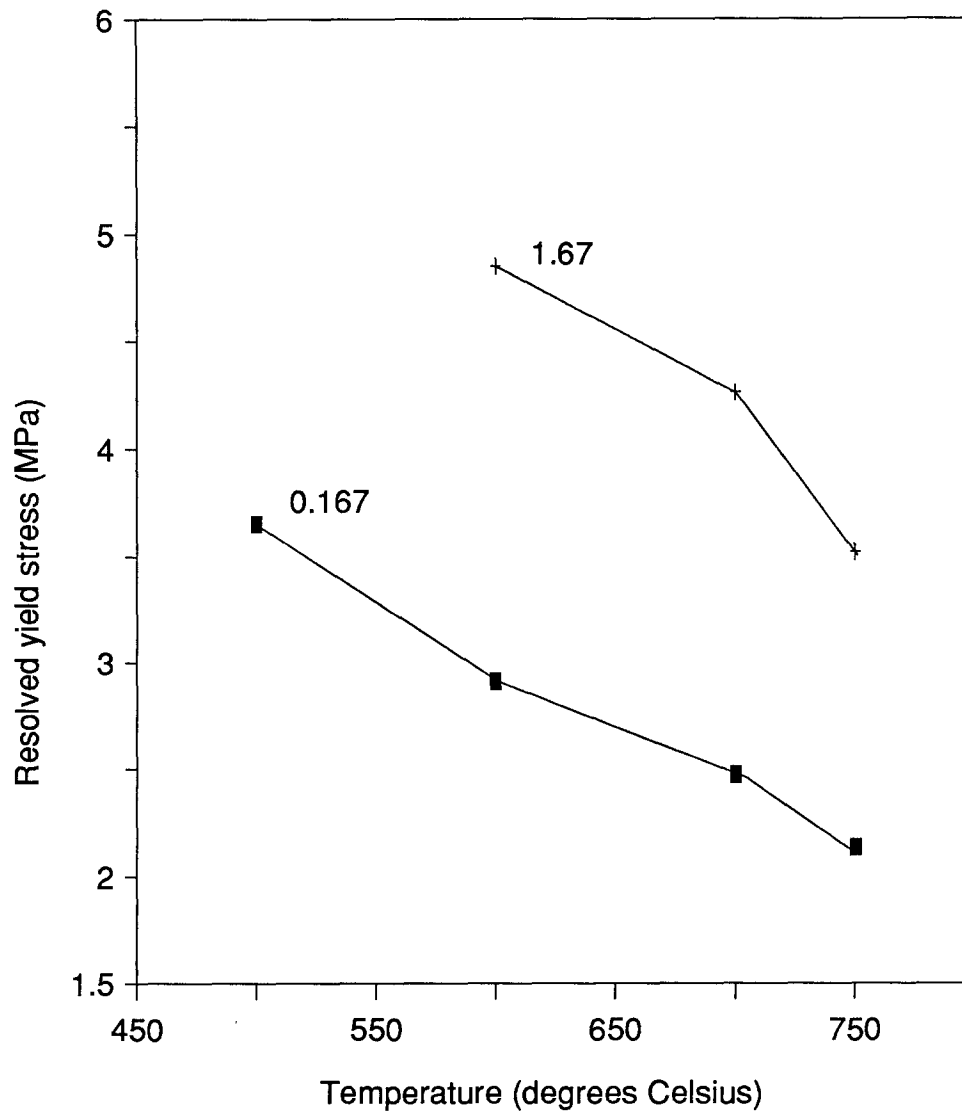


Fig 5.15 Resolved yield stress as a function of temperature for the strain rates indicated  $\times 10^{-4}/s$ .

Temp. °C	Sample	Yield stress (MPa)	$\tau_{III}$ MPa	$\Delta l$ (chart) mm	$\Delta l$ (sample) mm	Strain rate $\times 10^{-4}$ /s	CHS (cm/sec)
400	T1	F	F				$4.2 \times 10^{-5}$
	T2	F	F				$4.2 \times 10^{-4}$
	T3	F	F				$2.1 \times 10^{-3}$
500	T4	3.65	7.43	3.3	2.95	0.167	$4.2 \times 10^{-5}$
	T5	F	F				$4.2 \times 10^{-4}$
	T6	F	F				$2.1 \times 10^{-3}$
600	T7	2.91	5.66	3.73	2.74	0.167	$4.2 \times 10^{-5}$
	T8	4.85	10.25	5.1	3.68	1.67	$4.2 \times 10^{-4}$
	T9	F	F				$2.1 \times 10^{-3}$
	T10	F	F				$8.5 \times 10^{-3}$
700	T11	2.47	5.84	3.4	2.67	0.167	$4.2 \times 10^{-5}$
	T12	4.26	8.16	6.6	5.89	1.67	$4.2 \times 10^{-4}$
	T13	F	F				$2.1 \times 10^{-3}$
	T14	F	F				$8.5 \times 10^{-3}$
750	T15	2.13	6.57	3.89	2.97	0.167	$4.2 \times 10^{-5}$
	T16	3.52	7.34	2.46	1.63	1.67	$4.2 \times 10^{-4}$

Table 5.7 Measured values of the yield stress, the recovery stress, the chart and sample elongations for the temperatures and CHS indicated (F = Samples fractured during elastic deformation).

### 5.2.3 Dislocation Density - Tensile Tests.

The dislocation densities in the tensile samples were estimated following the same procedure used for the compression test samples. The appearance and distribution of etch pits in an as received tensile sample is shown in Fig. 5.16 which as expected, is similar to that of the compression test sample. The pits are hexagonal and tend to overlap in clusters. The etch pit density in an as received sample was estimated to  $1.2 \times 10^4 / \text{cm}^2$ . The deformed samples when etched in KOH did not produce the well defined faceted pits as in the sample before deformation. An example of a deformed etched surface for a test temperature of  $500^\circ\text{C}$  and strain rate of  $1.67 \times 10^{-4} / \text{s}$  is shown in Fig. 5.17. The pits are small and without clearly defined facets. Some have shiny bottoms, others, dark bottoms. The density of the etch pits was estimated to be  $2.86 \times 10^6$  pits/ $\text{cm}^2$ .

Increasing the test temperature to  $600^\circ\text{C}$ , and etching the samples after deformation produced small etch pits similar to those obtained at  $500^\circ\text{C}$ . Examples of samples tested at  $600^\circ\text{C}$  at strain rates of  $1.67 \times 10^{-4}$  and  $8.33 \times 10^{-4} / \text{s}$  are shown in Figs. 5.18 and 5.19. The etch pit densities were estimated to be  $6.91 \times 10^5$  and  $1.04 \times 10^6$  pits / $\text{cm}^2$  respectively. The results of the etch pit density measurements are listed in Table 5.8.

Temp.°C	Sample	$\sigma_A - \sigma_Y$ (MPa)	$\epsilon_p$	strain rate $\times 10^{-4}/s$	Estimated etch pit density /cm <sup>2</sup>	Observed etch pit Density /cm <sup>2</sup>
500	T5			1.67		$2.86 \times 10^6$
600	T7	1.84	0.424	0.167	$1.94 \times 10^7$	$2.8 \times 10^7$
600	T8	9.76	0.507	1.67	$1.65 \times 10^7$	$6.91 \times 10^5$
600	T9			8.33		$1.04 \times 10^6$

Table 5.8 Dislocation etch pit density in deformed tensile samples,  $\sigma_A - \sigma_Y$  is the difference between the final stress in the sample and the yield stress,  $\epsilon_p$  is the plastic strain in the sample.

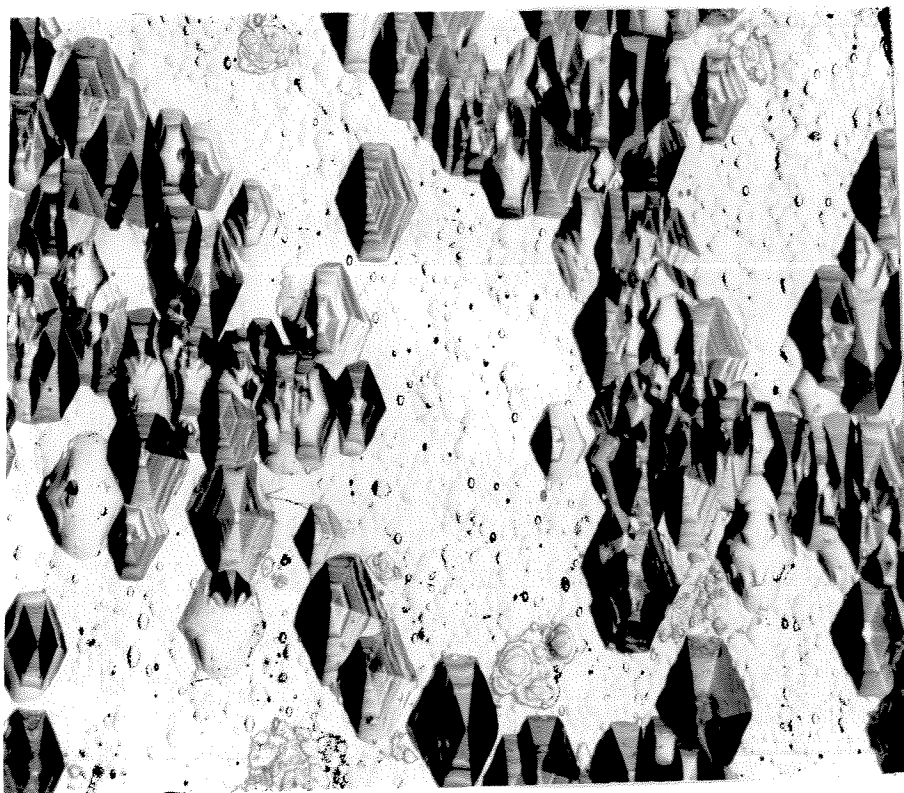


Fig 5.16 Dislocation etch pits in an as received GaAs wafer. Etching time was 10 minutes. Magnification X 175.

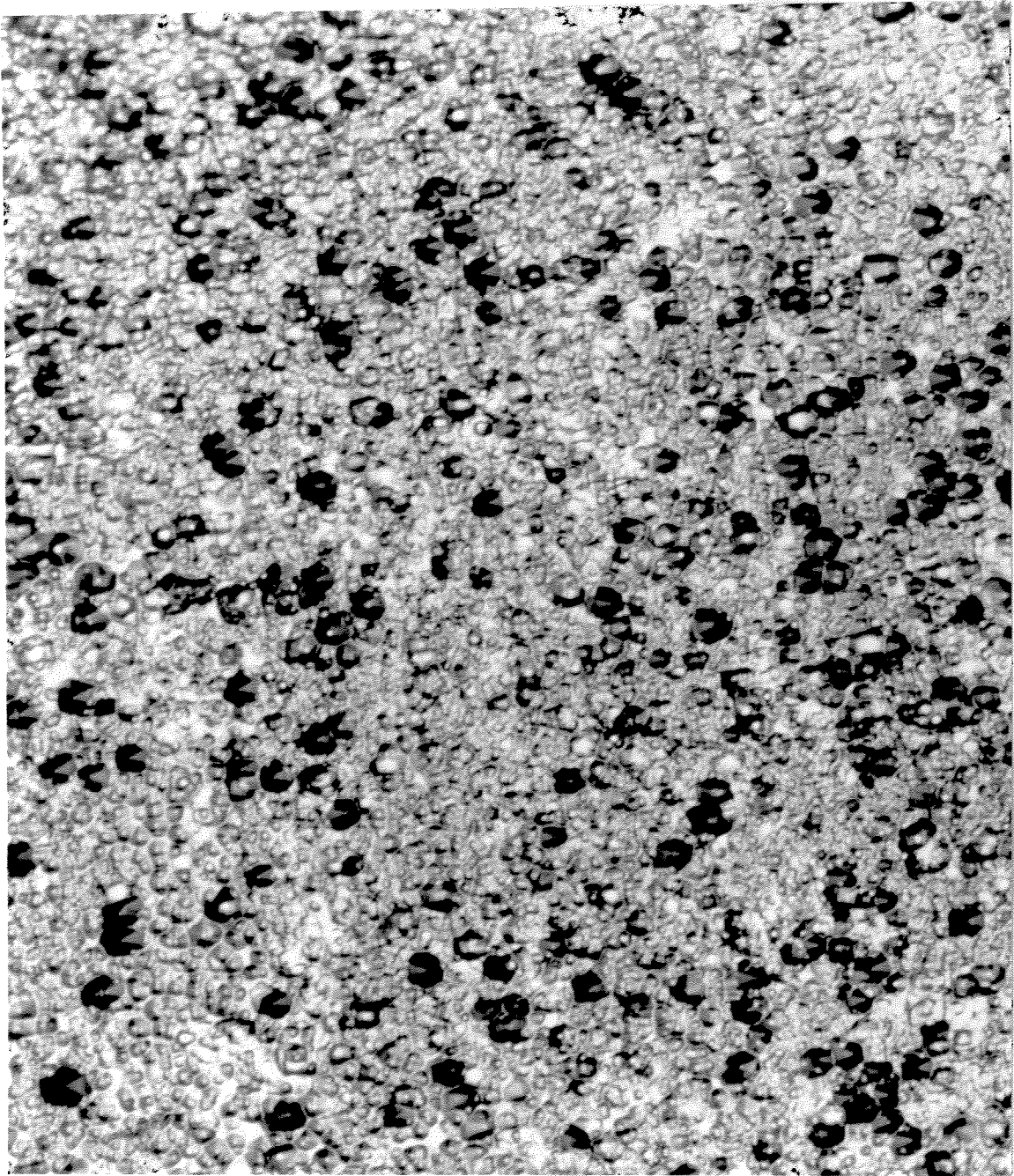


Fig 5.17 Dislocation etch pit density in a deformed GaAs wafers.(strain rate =  $1.67 \times 10^{-4}$ /s, test temperature =  $500^{\circ}\text{C}$ ). Magnification X 865, Sample number T5.

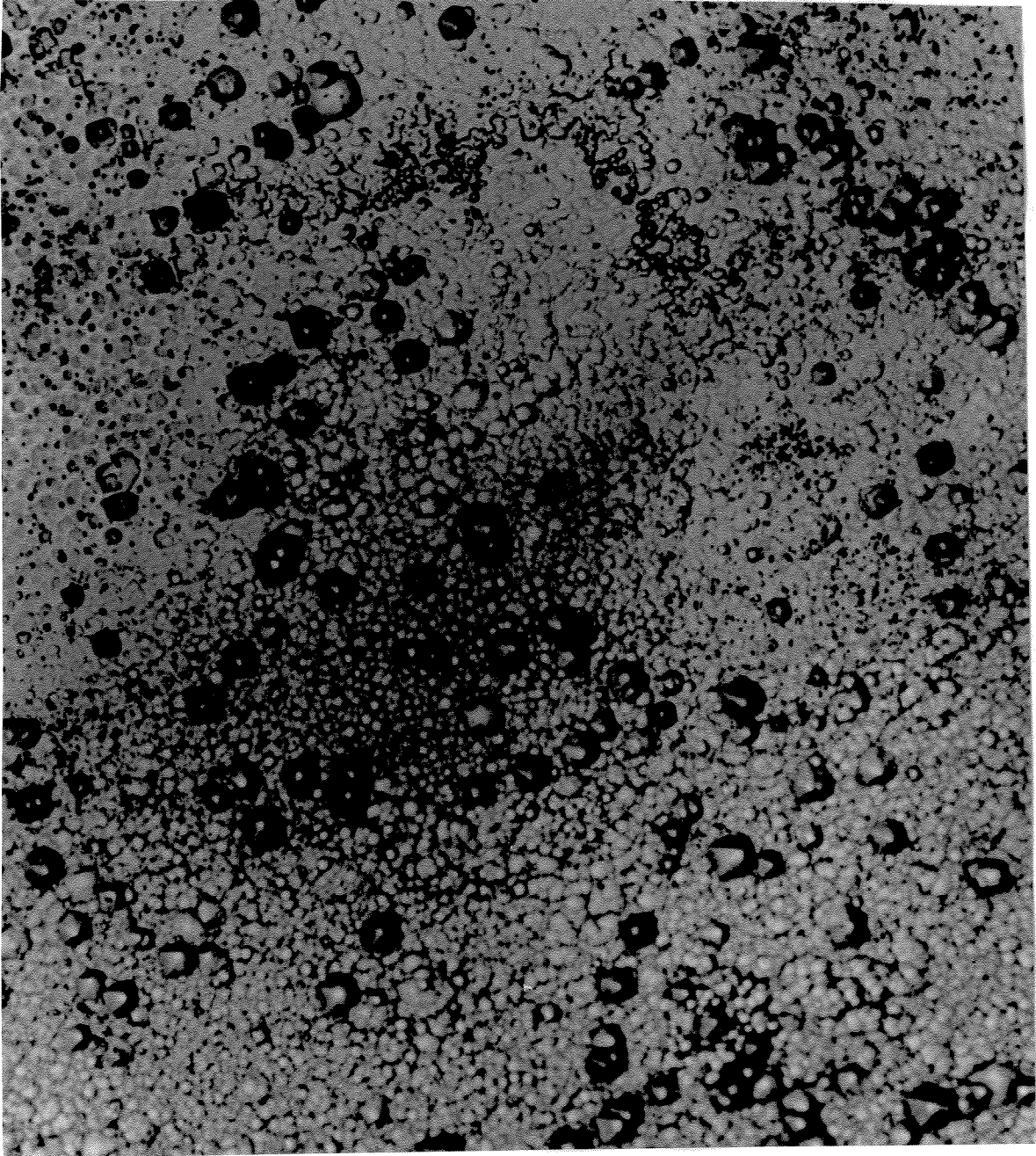


Fig 5.18 Dislocation etch pit density in a deformed GaAs wafer.(strain rate =  $1.67 \times 10^{-4}$ /s, test temperature =  $600^{\circ}\text{C}$ ). Magnification X 427, Sample number T8.

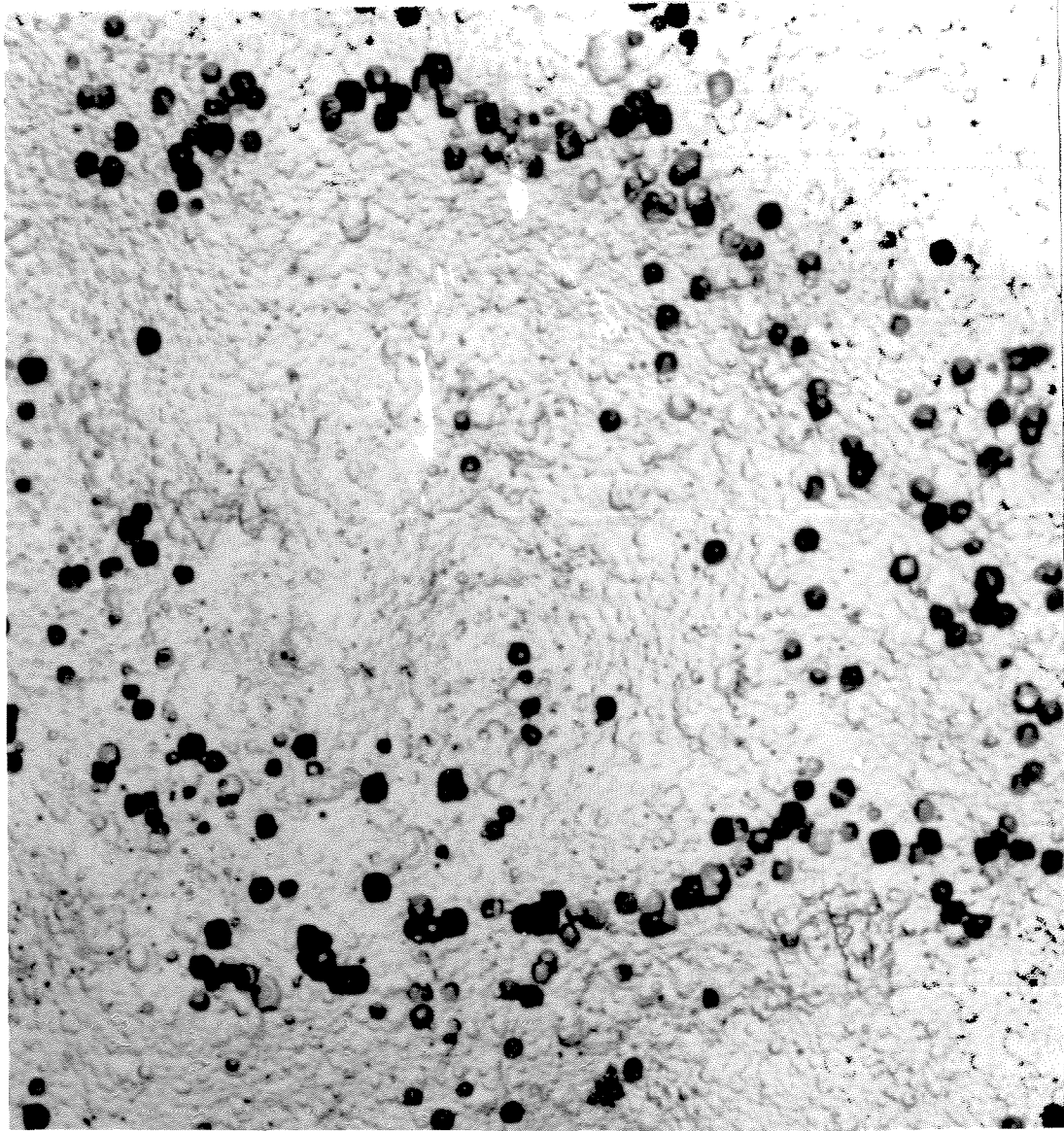


Fig 5.19 Dislocation etch pits in a deformed GaAs wafer (strain rate =  $8.33 \times 10^{-4}$  /s, test temperature =  $600^{\circ}\text{C}$ ). Magnification X 968, Sample number T9

## 6

**DISCUSSION**

There exists in the literature, conflicting reports on the magnitude of the parameters characterising the beginning of plastic deformation of GaAs and also on the temperature and strain rate dependence of these parameters. Most of the values reported were obtained within a narrow range of temperature and this makes it difficult to resolve the differences in the reported values. Also most of the results reported were for specimen orientations favourable to single slip and the stress - strain curves showed a pronounced yield drop. It was thus widely claimed that the yield drop phenomena is a typical feature of the stress - strain curves of GaAs. The temperature, stress and strain rate dependence of the dislocation density in deformed GaAs specimens have also been a subject of strong interest. This research was directed toward finding a link between the results reported in the literature, and to observe the relation between the dislocation density and deformation variables. An explanation of the results obtained in the present study and those reported in the literature was sought on the basis of the microscopic theory of dislocations.

It was found in the course of the experiments that preparation of the test samples and deforming the GaAs at high temperatures was more difficult than anticipated. GaAs is highly brittle at low temperatures, resulting in sample failure during sample preparation. Compression samples were made from seed crystals provided by Johnson Matthey, since cutting facilities were not available, The internal strains in the crystals provided and the overall quality were not clearly defined. Etching the deformed samples for delineating dislocations was difficult and non reproducible, which makes the observations of the etch pit density partly ambiguous. Edge grinding of the tensile samples also proved difficult due to sample breaking during grinding or during handling for cleaning and fitting into the tensile grip system.

## 6.1 Yield Drop.

The stress - strain curves for both the compression and tension tests show a smooth transition from elastic to plastic deformation. No yield drop was observed in all the experiments. The yield drop phenomena has been a subject of increasing controversy and a number of theories have been proposed to explain the phenomena.

The yield drop phenomena has been accounted for in terms of the amount of initial and potentially mobile dislocations that are present in the specimen prior to deformation. In this theory, the application of an external stress causes the generation of dislocations which adds a plastic term to the applied strain rate. The elastic term thus decreases while the plastic term increases. The stress then goes through a maximum (upper yield point) and may even fall to zero were it not for work hardening which limits the multiplication of dislocations and allows the stress to rise again. (lower yield point). In agreement with this model, the magnitude of the yield drop decreases with increasing temperature and the extent of pre - strain present in the sample prior to deformation.

The yield drop has also been explained in terms of Cottrell's theory where it is associated with an unpinning stress. In this theory, the dislocations are considered to be surrounded by impurity atmospheres which pins them strongly to the lattice. The stress required to unpin these dislocations from the atmospheres is then assumed higher than the stress they require to move through the lattice, hence the yield drop. This theory has been used to explain the yield drop phenomena in many metals (29).

In GaAs, the grown - in dislocations do not move under an applied stress (6) and their role as sources of new dislocations remains unclear. The parabolic stress - strain curves obtained

in the present study are then associated with the activation of multiple slip systems which generates a high dislocation density prior to yielding. The result is that changes in the dislocation density before and after yielding and thus changes in the dislocation velocity are not significant and this suppresses the yield drop.

## 6.2 Temperature and Strain Rate Dependence of $m$ and $U$ .

The temperature and strain rate dependence of  $m$  and  $U$  may be correlated directly to the temperature and strain rate dependence of the dislocation types that are effectively present and active during the deformation process. Two pertinent questions arise.

1. What dislocation types are present in the crystal during the deformation process and which are rate controlling.?
2. What is the temperature and strain rate dependence of  $m$  and  $U$  for these types of dislocations.?

Recent experiments on dislocation velocities in semiconductors (16,17,30,31,32,33) have shown a stress dependence of the dislocation velocity below a specific critical stress which depends on the crystal and also on the dislocation type. Below this stress, the resulting velocity equation may not be properly described by a simple power law. In germanium for example, the results of velocity measurements show that for  $60^\circ$  dislocations, a plot of the log of the dislocation velocity versus the log of the applied stress is linear for applied stresses above  $2\text{kp/mm}^2$  while for stresses below  $2\text{kp/mm}^2$ , the curves show a large and temperature dependent slope. (30,33). Similarly for silicon, the activation energy of the  $60^\circ$  dislocations and the stress exponent are stress and temperature dependent respectively for stresses below  $3\text{kp/mm}^2$ . However the results for screw dislocations show the activation energy and the stress exponent to be stress and temperature independent respectively for stresses greater than  $0.4\text{kp/mm}^2$  (11,30,35).

It is this breakdown in the power law equation that is responsible for the apparent confusion in the literature on the "correct" magnitudes of  $m$  and  $U$  obtained from experiments performed at different temperatures and strain rates. In the temperature and stress interval in which dislocation velocities have been measured in GaAs (16),  $\beta$  dislocations were shown to have the lowest mobility compared to  $\alpha$  and screw dislocations hence their motion was thought to be rate controlling. However the absolute values of the activation energy obtained in

macroscopic deformation experiments differed from the activation energy of any of the individual dislocation types. The results of Steinhardt and Haasen (18) on the creep rates of GaAs indicates that the average creep rate depends on some suitable combination of the velocities of the different dislocation types. It was shown in that study that the macroscopic activation energy should be defined by

$$U = \frac{1}{2}(U_{\alpha} + U_s) \quad [21]$$

where  $U_{\alpha}$  and  $U_s$  are the activation energy for the  $\alpha$  and screw dislocations respectively. Recently, Rabier and Boivin (5), have shown that the density of screw dislocations in a deformed GaAs specimen depends on the deformation temperature. In that study, they showed that at low temperatures, the deformation substructures of GaAs single crystals consists mainly of screw dislocations while at high temperatures, the substructure shows a low density of screw dislocations. The transition from a substructure where the density of screw dislocations is low to one where it's density dominates was explained in terms of the temperature dependence of the activation energy of cross slip. At high temperatures, the activation energy is low, hence cross slip takes place readily and opposite screw segments annihilate each other. At low temperatures, cross slip is more difficult to activate and this leads to an accumulation of screw dislocations in the primary glide plane. Thus the contribution of screw dislocations to the total dislocation density and hence to strain hardening depends on the test temperature. It is this problem related to the crystal structure of GaAs that limits the comparison of  $m$  and  $U$  obtained at different temperatures and strain rates.

The present results show that the magnitude of  $(2+m)$  is temperature dependent with values ranging from 3.33 at 400°C to 3.96 at 800°C. while changes in the values of the activation

energy obtained in the present study are not so pronounced. This variation in the magnitudes of  $(2+m)$  from 400°C to 800°C. is qualitatively in agreement with the temperature dependence of the rate sensitivity of the flow stress at high temperatures obtained for ZnS (34). In ref (34), the stress sensitivity of the strain rate increased with temperature in the temperature range of about 200°C to 370°C before decreasing with temperature down to 540°C.

The present results are not in agreement with that of Schroter et al on germanium. (25). They report that  $m$  decreased with increasing temperature. It was also shown in ref (25) that while  $m$  and  $U$  depends on temperature and strain rate respectively for germanium,  $m$  and  $U$  does not show the same dependence in silicon.

In comparison with macroscopic deformation experiments, the results of dislocation velocity measurements show that only the velocity of screw dislocations may be described approximately by the simple power law relation of equation [6] for all the stress intervals presently investigated. The discrepancies in the results of macroscopic deformation experiments may then be explained in terms of the stress and temperature dependence of dislocation types whose motion is rate controlling. In Ge  $60^\circ$  dislocations have been shown to be rate controlling (12) while for Si the motion of screw dislocations are rate controlling.(11). The temperature and stress dependence of  $m$  and  $U$  for germanium compares favourably to the temperature and stress dependence of the  $60^\circ$  dislocations in germanium while the constant values of  $U$  and  $m$  for silicon may be due to the fact that no asymmetry has been observed in the temperature and stress dependence of the velocities of screw dislocations (32,35) . It has been suggested that this may be due to it's strong covalent bonding which induces a very high Peierls stress. The scatter in the values of  $U$  and  $(2+m)$  obtained in the present results and also in those listed in Table 5.4(b) may be associated with structural changes that occur in the specimens during plastic deformation and due to the large temperature and strain rate variations not allowed for

in the equations derived by Haasen (2). The assumption of a constant activation energy for the parameters characterising the beginning of plastic deformation implicit in the model presumes that dislocations are driven mainly by a single mechanism at all temperatures and strain rates.

The effect of thermal activation on the generation and motion of dislocations and hence in the plastic flow of metals is seen in the precipitous rise of the yield stress of most of the refractory b.c.c. metals (iron, tungsten, tantalum etc.) on decreasing the deformation temperature below room temperature. This result has also been observed both for single and poly-crystalline materials and is thus not attributable to the presence of grain boundaries. On defining the deformation stress as the stress that causes the dislocations to move a large distance compared to their mean separation, these results indicate that the deformation stress is a sum of two terms, a plastic term and a thermal term. For any given structure and specimen orientation, the deformation stress is constant. Thus for the same strain rate and temperature, repetitive experiments using identical specimens will produce the same yield stress. (the plastic component of the deformation stress). On changing either the strain rate or the deformation temperature, we change not the deformation stress but its components. Increasing the temperature increases the thermal term while reducing the plastic term. This is manifested by a reduced yield stress. Increasing the strain rate increases the plastic term while reducing the thermal term and hence an increased yield stress.

The agreement of the experimental results with the equations of Haasen's model at low temperatures and high strain rates arises because under these conditions, the thermal component of the deformation stress is not significant, consequently the dislocations in the specimen are driven mainly by a single mechanism, in this case the applied stress. On increasing the temperature or reducing the strain rate, we obtain a gradual transition from plastic to viscous deformation, for then, localised obstacles to the dislocations may be overcome purely by thermal fluctuations and also the diffusion of point defects contributes significantly to the plastic flow.

All of these processes, in addition to the applied stress, compete effectively for the rate controlling mechanism and consequently, equation [11] ceases to be a correct description of the stress and temperature dependence of the plastic strain rate and this limits the validity of the results obtained using this model under these conditions.

The critical stress dependence of the dislocation velocity below which the power law relation breaks down may be associated to a transition from a single mechanism controlled deformation to a multi - mechanism controlled deformation. Thus this critical stress defines the transition stress above which the equations of Haasen's model holds. Below this stress, the equations of the model have to be modified to account for the contributions of temperature induced effects to the plastic strain rate.

## 6.3 Stress - Strain Curves.

### 6.3.1 Compression Tests.

The general shape of the compression stress strain curves shown in Fig. 5.1 is consistent with similar results reported in the literature (36,37). The magnitude of the yield stress observed in the present investigation drops appreciably with test temperature and varies with strain rate (Table 5.2(a)). The present results of the compressive resolved yield stress of GaAs are compared to reported values in Table 5.9. At 700°C and for roughly similar strain rates, the measured yield stress is 4.08 MPa compared to the reported value of 2.8 MPa, At other temperatures, the measured values are also appreciably higher than the reported values.

The high values of the yield stress obtained in the present study are difficult to account for. It is possible that they are associated with the condition of the test samples. The samples were cut from seed crystals with a diamond saw. The seed crystals themselves were cut from a large crystal boule with a diamond saw. As a result all the sample surfaces were cut and in the process of cutting, internal strains may have developed in the samples. It is not clear whether these strain were alleviated at the test temperatures prior to deformation. The samples were not annealed at high temperatures due to the potential loss of arsenic by evaporation. Internal strains could lead to higher yield stress. We note that at the highest test temperature (800°C) and lowest strain rate ( $0.33 \times 10^{-4}$ /s), the yield stress drops to 1.53 MPa. appreciably lower than the value at the higher strain rate. The present high values of the yield stress are thus attributed to internal strains in the starting material which could not be eliminated in a controlled manner. There was no other manner of preparing samples in the present investigation.

In the present study, for test temperatures of 500°C, plastic deformation was observed with some recovery (stage III) at high stress values. This differs from reports (15) that stage III may not be observed below 550°C prior to fracture.

Temp°C	Strain rate x 10 <sup>-4</sup> /s.	Orientation	Present Results MPa	Reported Results MPa
600	1.67	[100]	5.51	
	not stated	[100]		6.9
700	1.67	[100]	4.08	
	1.0	[100]		2.80
800	1.67	[100]	3.47	
900	1.0	[100]		2.45

Table 5.9 Comparison of present results with values reported in the literature, ref(37).

### 6.3.2 Tension Tests.

The values of the resolved yield stress for GaAs, given in Table 5.7 are shown to vary appreciably with temperature and strain rate similar to that observed in the compression tests. In a number of samples, as indicated, fracture occurred before the onset of plastic deformation, particularly at the higher strain rates and lower temperatures. This is a reflection of the brittle characteristic of GaAs at lower temperatures. Comparing the yield stress of the tensile samples with the compression samples (Tables 5.7 and 5.2(a)), It is observed that for the lower test temperatures, the values in tension are below that observed in compression. At the slowest strain rates, comparing tension and compression values of 3.65 and 4.29 MPa at 500°C, 2.91 and 3.27 MPa at 600°, 2.47 MPa and 2.04 MPa at 700°C. The difference decreases at the higher temperatures. In general, it is assumed that the resolved yield stress in tension and compression should be the same. It is not clear why the difference is observed in the present case. It is postulated that the compression test samples contain internal strains prior to deformation. The tension tests samples have polished faces and were chemically polished after careful shaping which likely eliminates or markedly reduces internal strains and this could account for the difference.

In Table 5.7, the increase in length of the tensile gauge length at fracture  $\Delta l$  as determined from the Instron chart is compared to  $\Delta l$  measured from the sample after fitting the fractured pieces together as carefully as possible. The measured lengths of the fractured samples are consistently smaller than the chart values by between 10 and 30 %. This indicates that tensile strains are introduced during testing in addition to the strains in the sample. This then accounts for the shallow slope of the elastic portion of the stress strain curves and makes quantitative evaluation of stress strain curves in which strain plays a significant role uncertain.

A direct comparison of the resolved yield stress in tension between the present results and reported values cannot be made since values for GaAs of [100] orientation at high temperatures have not been reported.

Also, a more detailed comparison of the stress strain curves determined in this investigation with the plastic deformation model as proposed by Haasen (2) appears to be of limited value. The strains measured, only approximate the actual strains produced in the sample. In addition the temperature and strain rate dependence of the flow stress is required. As reported in Table 5.7, all of the samples deformed at strain rates higher than  $1.67 \times 10^{-4}$  /s fractured during elastic deformation . The strain rate dependence of the flow stress thus cannot be determined from the present data.

### 6.3.3 The Relation Between The Dislocation Density and Macroscopic Deformation Variables.

The relation between the dislocation density in a deformed specimen and the macroscopic deformation variables has been a subject of strong interest. In the investigation of the high temperature deformation of GaAs by bending (6), it was shown that a marked increase in dislocations occurred after small strains. The dislocations were detected using cathodoluminescence. It was also demonstrated in undeformed GaAs that there is a direct correlation with etch pits and dislocations on (100) surfaces of GaAs.

Without assuming any definite mechanism for the multiplication of dislocations, it seems reasonable to assume that there exists a functional relation between the dislocation density in a deformed specimen to the applied stress, the strain rate, the plastic strain and the deformation temperature. This functional relation is expressed empirically below.

$$\rho = k \Delta\sigma^a \dot{\epsilon}^b \epsilon_p^c T^d \quad [22]$$

where  $k$ ,  $a$ ,  $b$ ,  $c$  and  $d$  are constants to be determined. In the above equation,  $\Delta\sigma$  is taken to be the difference between the applied stress and the yield stress of the specimen while  $\dot{\epsilon}$ ,  $\epsilon_p$ , and  $T$  are the strain rate, plastic strain and deformation temperature respectively. The physical question then is at what point during the plastic deformation of a crystal do the dislocations begin to significantly multiply. The results of dislocation experiments (41,42) indicate the existence of a threshold stress. In this study, this threshold stress was taken to be the yield stress of the specimen.

The constants in equation [22] were determined from the present data. Values of the parameters were substituted in the equation and using Newton's method, the equations were

differentiated with respect to each of the variables and the resulting equation solved for the constant terms. On this basis the functional relation between the dislocation density and the deformation variables was found to be

$$\rho = \frac{3988. \Delta\sigma^{0.023} \epsilon_p^{0.081} T^{1.32}}{\dot{\epsilon}^{0.093}} \quad [23]$$

This result show that the dislocation density is directly related to the applied stress, the plastic strain in the specimen, and the deformation temperature while being inversely related to the strain rate ( a lower strain rate being equivalent to an increased temperature).

Values of the dislocation density for a range of temperatures and strain rates were calculated from the test variables giving the results shown in Table 5.6. The experimental observations of the etch pit dislocation density after plastic deformation in compression are also listed in Table 5.6. Assuming the small pits to be associated with dislocations arising from plastic deformation and the large pits with grown in dislocations in GaAs. The observed small pits are compared to the calculated dislocation etch pit density.

The values for the etch pit dislocation densities from the tensile test samples are listed in Table 5.8. Using the constants from the compression tests data, values of the dislocation densities were calculated using two tensile tests data and the results compared with the measured values in Table 5.8.

## 7

**Conclusions**

1. The stress and temperature dependence of the activation energy ( $U$ ) for the generation of dislocations and the stress exponent ( $m$ ) of the dislocation velocity obtained from macroscopic deformation experiments correlates directly to the stress and temperature dependence of the dislocation types whose motions are rate controlling.

2. Haasen's model of plastic deformation is not applicable to GaAs in the temperature range (400°C - 800°C) investigated in the present study.

3. The critical stress dependence of the dislocation velocity below which the power law equation breaks down, marks a transition stress above which the deformation model of Haasen holds.

4. The differences in the various values of  $U$  and  $m$  reported in the literature are not due to experimental errors as has been claimed, but are due to the different temperatures and strain rates under which the results were obtained.

5. The dislocation density in a deformed GaAs sample is directly related to the applied stress, the plastic strain and the test temperature while being inversely related to the applied strain rate.

## 8

**SUGGESTIONS FOR FURTHER WORK**

Haasen's model of plastic deformation remains the most consistent dislocation model for diamond structure materials. However, at high temperatures the model has to be modified to account for the contributions of temperature to the plastic strain rate.

The process of this modification may be aided by finding answers to the following basic questions.

What processes contribute to the plastic strain rate at high temperatures

How can we describe the contributions of each of these processes quantitatively.

How do these processes relate to each other. For instance are they parallel dependent or independent processes etc.

The fact that the constants  $B(T)$ ,  $A$ ,  $K$ , in the equations of the model are not known for GaAs limits the application of the model to GaAs. The constant  $A$  may be obtained using equation [5] as follows

$$\sigma_A = \sigma_{eff} + AN^{\frac{1}{2}}$$

Thus a plot of  $\sigma_A$  Vs  $N^{1/2}$  should give a straight line whose slope is  $A$ . The temperature dependence of  $A$  may also be examined in the same experiment.

With  $A$  known,  $K$  may be obtained by re-writing equation [9] as

$$dN = NK\sigma_{eff}Vdt$$

By using equation [2] , the above equation reduces to

$$\frac{dN}{d\varepsilon} = \frac{K}{b} \sigma_{eff}$$

Thus by plotting the ratio of the change in dislocation density to the corresponding change in strain for a given effective stress, K could be determined.

The determination of B(T) is more difficult experimentally. However the problem may be resolved if A and K are known. Then equations [9] and [10] may be treated as boundary value problems and a B(T) found such that the theoretical curve fits a given experimental curve.

**REFERENCES**

- 1 P. B. Hirsh, *Materials Science and Technology*. sept. 1985. vol 1, p666
- 2 H. Alexander and P. Haasen, *Solid State Physics* vol 22, 1968, p27.
- 3 F. Weinberg, *Transactions of the Matallurgical Society of AIME*. vol 242, Oct 1968, p2111.
- 4 F. Weinberg, *Canadian Journal of Physics*, vol 45, (1967), p1189.
- 5 J. Rabier and P. Boivin, *Philosophical Magazine A* 1990, vol 61 no4, p673.
- 6 P. J. Gallagher and F. Weinberg, *Journal of Crystal Growth*. vol 94, 1989 p299.
- 7 Ichiro Yonenaga and Koji Sumino, *Journal of Appl. Physics*. 62 (4), 15 august 1987.
- 8 J. Volkl and G. Muller, 5<sup>th</sup> conference on Semi - Insulating III - V Materials, Malmo, Sweden. 1988, p489.
- 9 T Alden, *Metallurgical Transactions A*. vol 18A, May 1987, p811.
- 10 Ken-Ichi Kojima and K. Sumino, *Crystal Lattice Defects*, vol 2, 1971, p147.
- 11 I Yonenaga and K. Sumino, *Phys. Status Solidi. A* ,vol 50, 1978, p685.
- 12 Koji. Sumino and Ken. - Ichi Kojima, *Crystal Lattice Defects* 1971, vol 2, p159.
- 13 Ichiro Yonenaga, Utako Onose and Koji Sumino, *Journal of Material Research* vol 2, no2, Mar/April 1987, P252.

- 14 P. Astie , J.J. Couderc , P. Chomel, D. Quelard and M. Duseaux, *Phys. Status Solidi A*, vol 96, 1986, p225.
- 15 Hans Siethoff , R. Behrensmeier, K. Ahlborn and J. Volkl, *Philosophical Magazine A*, 1990, vol 61, no2, p233.
- 16 V.B. Osvenskii, and L.P. Kholodnyi, *Soviet Physics-Solid State* vol 14, no 11, 1972, p2822.
- 17 V.B. Osvenskii , L.P. Kholodnyi and M.G. Mil'vidskii, *Soviet Physics-Solid State*, vol 15, no 3, 1973, p661.
- 18 H. Steinhardt and P. Haasen, *Physics Status Solidi A*, vol 49, 1978, p93.
- 19 V.B. Osvenskii, L.P. Kholodnyi and M.G. Mil'vidskii, *Soviet Physics- Doklady* vol 14, n0 2, 1969, p144.
- 20 V.B. Osvenskii, S.S. Shifrin and M.G. Mil'vidskii, *Soviet Physics- Crystallography*. vol 13, no 5, 1969, P718.
- 21 H. Steinhardt and S. Schafer, *Acta Metallurgica*, vol 19, (1971), P65.
- 22 P. Boivin, J. Rabier and H. Garem, *Philosophical Magazine A* vol 61, no 4 (1990), P619.
- 23 H. Gottschalk, G. Patzer and H. Alexander, *Physics Status Solidi A*, vol 45, (1978), P207.
- 24 M'Barek Omri, Jean-Pierre Michel and A. George, *Philosophical Magazine A*, vol 62, no 2,(1990), p203.

- 25 W. Schroter, Hans Georg Brion and Hans Siethoff, *Journal of Applied Phys.* vol 54,  
no 4 (1983), P1816.
- 26 T. H. Alden, *Mettallurgical Transactions A.* vol 16A, march 1985, P375.
- 27 S. Amelinckx, *Discussions of The Faraday Society*, no 38,, p7 (1964).
- 28 V. Swaminathan and S.M. Copley, *Journal of The American Ceramic Society*, vol 58,  
no 11 -12, p482.
- 29 W.G. Johnston, *Journal of Applied Physics.* vol 33, no 9 (1962), p2716.
- 30 H. Alexander, *Dislocations in Solids.* vol 7 1986, P115
- 31 F. Louchet , D Cochet Muchy and Y Brechet, *Philosophical Magazine A*, vol 57, no  
2, 1988, p327.
- 32 A. George, C. Escaravage, G. Champier and W. Schroter, *Physics Status Solidi B.* vol  
53, 1972, p483.
- 33 M. N. Kabler, *Physical Reveiw*, vol 131, no 1, 1963, p54.
- 34 Collete Levade, Jean-Jacques Couderc, Isabelle Dudouit and Jean Garigue,  
*Philosophical Magazine A*, vol 54, no2, 1986, p259.
- 35 Masato Imai and Koji Sumino, *Philosophical Magazine*, vol 47A, 1983, P599.
- 36 A. Djemel, J Castaing, *Europhysics Letters*, 2 (8), p611, 1986.
- 37 S. Guruswamy, R.S. Rai and K. T. Faber, *Journal of Appl Physics* 62(10), p4130,  
Nov. 1987.

- 38 M'Barek Omri , Claude Tete, Jean-Pierre Michel and A. George, Philosophical Magazine A, vol 55, no 5, 1987, p601.
- 39 S. Tohno amd A. Katsui, Defect Recongnition and Large Processing in III-IV Compounds II, Elsevier Publishers, B.V. Amsterdam, 1987,p87.
- 40 M. Fnaiech, F. Reynaud, A Couret and D. Caillard, Philosophical Magazine. A. 1987. vol 55. no. 4, p405.
- 41 Koji Sumino and Masato Imai, Philosophical Magazine A, vol 47, no 5 1983, p753.
- 42 A. Djemel, J. Castaing, N. Burle - Durbec and B. Pichaud, Revue Physics Appl, 24 (1989), p779.
- 43 S.K. Choi, M. Mihara, T. Ninomiya, Japan Journal of Applied Physics. vol 16, no 5, may 1977, p737.
- 44 V. Celli, M. Kabler, T Ninomiya and R Thomson, Physical Reveiw, vol 131, no1, 1963, p58.
- 45 H. Siethoff, Journal de Physique. Colloque C4. Supplement au 9, PC4-217, sept 1983.
- 46 H. M. Hobgood , S. McGuigan, J. A. Spitznagel and R.N. Thomas, Appl. Phys. Letters vol 48, no 24, 1986, p1654.
- 47 V. H. Schaumberg, Philosophical Magazine A, vol 25, p1429.
- 48 A.S. Krausz and B. Faucher, Reveiw on the Deformation Behaviour of Materials vol IV, no 2, 1982.

- 49 J.P. Hirth and J. Lothe, Theory of Dislocations. John Wiley and Sons, New York, 1982.
- 50 W.G. Johnston and J.J. Gilman, Journal of Applied Physics. vol 30, no2, 1959. p129.
- 51 D. Dew-Hughes, IBM Journal of Research, 1961, p279
- 52 T. H. Alden, Metallurgical Transactions A, vol 18A, Jan 1987, p51.